Article

Regulated control of gene therapies by drug-induced splicing

https://doi.org/10.1038/s41586-021-03770-2

Received: 6 February 2020

Accepted: 23 June 2021

Published online: 28 July 2021

Check for updates

Alex Mas Monteys[1,2]✉, Amiel A. Hundley[1], Paul T. Ranum[1], Luis Tecedor[1], Amy Muehlmatt[1], Euyn Lim[1], Dmitriy Lukashev[3], Rajeev Sivasankaran[3] & Beverly L. Davidson[1,2]✉

So far, gene therapies have relied on complex constructs that cannot be finely controlled[1,2]. Here we report a universal switch element that enables precise control of gene replacement or gene editing after exposure to a small molecule. The small-molecule inducers are currently in human use, are orally bioavailable when given to animals or humans and can reach both peripheral tissues and the brain. Moreover, the switch system, which we denote X^{on}, does not require the co-expression of any regulatory proteins. Using X^{on}, the translation of the desired elements for controlled gene replacement or gene editing machinery occurs after a single oral dose of the inducer, and the robustness of expression can be controlled by the drug dose, protein stability and redosing. The ability of X^{on} to provide temporal control of protein expression can be adapted for cell-biology applications and animal studies. Additionally, owing to the oral bioavailability and safety of the drugs used, the X^{on} switch system provides an unprecedented opportunity to refine and tailor the application of gene therapies in humans.

Although viral and non-viral approaches for gene therapies have undergone substantial advancement over the past twenty years, the major focus has been on the cargo-delivery system. For example, viral capsid evolution and engineering has improved the cell and tissue targeting of adeno-associated viruses (AAVs), and the landscape of cell targeting for lentiviruses has been expanded by using different envelopes in viral production. Additionally, lipid nanoparticles have been refined for improved uptake. However, the cargo itself—and more importantly the elements that control the expression from that cargo—have not received the same attention, although engineered promoters, riboswitches or other 3′ regulatory elements that restrict expression to certain cell types have advanced[1–4].

To address this gap, here we develop a method to finely control protein translation via a drug-inducible switch. The X^{on} system takes advantage of alternative RNA splicing[5], a mechanism that provides for RNA and protein diversity through the inclusion or exclusion of different protein-coding exons, parts of exons, and different 5′ and 3′ noncoding exons. By controlling alternative splicing, we can regulate which exons are spliced in (or out). Notably, the X^{on} switch does not require any foreign elements for regulation, but rather takes advantage of drugs that are orally bioavailable and in human use to induce the rapid inclusion of an exon containing a start codon. As such, the X^{on} system can be applied to any genetic element of interest in cells or in animals.

Initially, alternative splicing for the regulated control of protein translation was achieved using drugs developed for the treatment of spinal muscular atrophy, a disorder that is caused by reduced levels of SMN1. The rationale is as follows: *SMN2*, a pseudogene of *SMN1*, is correctly spliced only around 10% of the time, resulting in an SMN2 protein that is functionally equivalent to SMN1[6]. Two drugs, LMI070 and RG7800/RG7619, can improve the proportion of correct *SMN2* splicing, and both show efficacy in animal models of spinal muscular atrophy[7,8]. Notably, these drugs are in later-stage clinical testing (LMI070)[9] or have been approved for use in humans (RG7800/RG7619)[10].

Our first derivation of a splicing switch for controlled translation used a modified *SMN2* minigene, such that exon 7 (e7) exclusion and premature termination would occur in the absence of drug, but e7 inclusion and in-frame gene expression would occur in the presence of splice modifiers (Fig. 1a). For this, the original minigene was modified at the e7 acceptor splice site to reduce the approximately 10% background splicing in the native condition (indSMN2; Extended Data Fig. 1a, b). IndSMN2 was further evaluated in response to various doses of LMI070 or RG7800. Both drugs induced e7 splicing, with a complete splicing switch evident at concentrations greater than 1 μM (Extended Data Fig. 1c). For indSMN2 plus LMI070, there was an approximately 20-fold induction (Fig. 1b, Extended Data Fig. 1d). LMI070 showed greater induction activity than did RG7800 (Extended Data Fig. 1c), possibly reflecting their different mechanisms. RG7800/RG7619 binds to the SMN2 pre-mRNA sequence and promotes a conformational change that increases e7 splicing activator affinity, whereas LMI070 stabilizes U1 small nuclear RNA interactions at the e7 5′ splice site[8,11].

Because the fully spliced-in switch required drug doses that are unlikely to translate to the clinic, we searched for exons for which splicing was responsive to therapeutically relevant conditions. HEK293 cells were treated with 25 nM LMI070 for 12 h, and RNA sequencing (RNA-seq) was performed to determine alternatively spliced exons that were present only under drug-treated conditions. Reads were aligned to the genome and splicing events that were exclusive to the LMI070-treated samples were identified. After LMI070 treatment, 45 drug-induced

[1]Raymond G. Perelman Center for Cellular and Molecular Therapeutics, The Children's Hospital of Philadelphia, Philadelphia, PA, USA. [2]Department of Pathology and Laboratory Medicine, University of Pennsylvania, Philadelphia, PA, USA. [3]Neuroscience Disease Area, Novartis Institutes for BioMedical Research (NIBR), Cambridge, MA, USA. ✉e-mail: monteysam@chop.edu; davidsonbl@chop.edu

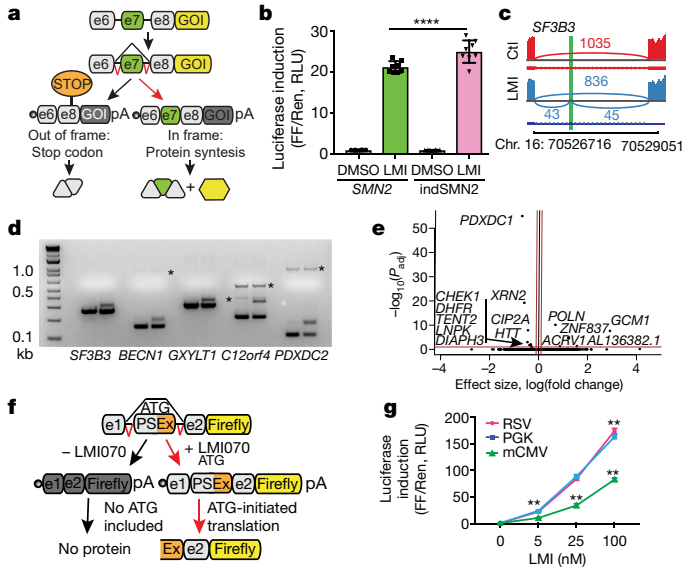

Fig. 1 | Generation and testing of X^{on}. a, Schematic depicting the SMN2-on cassette. In the absence of exon 7 (e7), a premature stop codon blocks translation of the gene of interest (GOI). Inclusion of e7 permits translation. **b**, Change in firefly (FF) luciferase activity in LMI070-treated (100 nM) compared with DMSO-treated cells, normalized to *Renilla* (Ren) luciferase activity. RLU, relative light units. Data are mean ± s.e.m. of 8 biological replicates, ****$P < 0.0001$ SMN2 versus indSMN2, two-way ANOVA, Bonferroni's post-hoc test. **c**, *SF3B3* splicing without (red; control (Ctl)) or with (blue) 25 nM LMI070 treatment. The genomic location of the LMI070 spliced-in *SF3B3* exon (green bar) and intron counts are indicated. **d**, cDNAs for *SF3B3*, *BECN1*, *GXYLT1*, *C12orf4* and *PDXDC2* amplified from cells treated with DMSO or LMI070 (25 nM) (one representative plot from 4 RNA-seq samples). Novel splicing was confirmed by Sanger sequencing. The asterisks represent non-specific bands. **e**, Volcano plot illustrating differentially expressed genes between DMSO-treated and LMI070- treated cells. The red horizontal bar represents 0.05 significance on a $-\log_{10}$ scale. The red vertical bars indicate thresholds of −0.1 and 0.1 fold change. Genes meeting the significance and minimum fold-change thresholds are labelled (4 samples per group). **f**, Candidate minigenes for translation control; e1 and e2 are the flanking exons of the novel *SF3B3* exon (Extended Data Tables 1, 2). **g**, Induction of luciferase activity in cells transfected with the *SF3B3*-based X^{on} cassette. Samples are normalized to *Renilla* luciferase and are relative to DMSO. Data are mean ± s.e.m. of 8 biological replicates, **$P < 0.01$ mCMV versus RSV or PGK; **$P < 0.01$ RSV versus PGK, two-way ANOVA followed by Bonferroni's post hoc test.

splicing events were above our threshold (an average of more than five novel intron-splicing events in LMI070-treated samples; Extended Data Tables 1, 2). Among them, 23 were exclusive to LMI070-treated samples and 22 were identified in all treated samples and were below our threshold criteria in control samples. To assess exclusivity, we queried the 45 events in a resource containing all exon–exon junctions from 21,504 human RNA-seq datasets (Methods). Using *SF3B3* as an example, the canonical exon–exon junction in *SF3B3* was observed in 12,872 datasets at an average frequency of 64 counts, whereas the LMI070-induced exon was observed in 10 and 1 dataset(s), respectively, for the 5′ and 3′ exon–exon junctions (Fig. 1c, Extended Data Tables 1, 2). The average counts per dataset for the 5′ exon–exon junction was 1.3, whereas the 3′ exon junction was observed only once. Thus, the LMI070-induced *SF3B3* exon almost never occurs naturally.

The candidate exons from LMI070-treated samples share a strong 3′ AGAGUA motif that is consistent with the identified LMI070-targeted U1 RNA binding site[8] (Extended Data Fig. 2a). The top five novel LMI070-induced splicing events were validated by PCR, which amplified the novel exons exclusive to cDNA samples from LMI070-treated cells (Fig. 1d). The global effect of LMI070 treatment on gene expression was also evaluated by differential expression analysis. There were 6 upregulated and 24 downregulated genes that passed the threshold for significance ($P < 0.05$; Benjamini–Hochberg multiple testing correction). After filtering out genes with low fold-change values (less than 0.1-fold) five upregulated and nine downregulated genes were identified (Fig. 1e).

We next used our custom pipeline to re-analyse a previous RNA-seq dataset[8] obtained from human cells treated with 100 nM LMI070. We observed strong concordance with our results, detecting 70% of our candidate genes in this previous dataset. The *SF3B3* and *BECN1* exons were the most significantly alternatively spliced in both datasets (Extended Data Fig. 2b, c). In addition, only 7 of the 42 reference splice events[8] induced by LMI070 were significantly differentially expressed in our study (Benjamini–Hochberg adjusted *P* value (P_{adj}) < 0.05; Extended Data Table 3), probably because of the low LMI070 concentration used here.

We developed switch-on luciferase cassettes using the minimal intronic intervening sequences to recapitulate splicing of the drug-responsive pseudo exons in *SF3B3*, *BECN1*, *C12orf4* and *PDXDC2*. To limit translation such that it would occur only in response to the drug, the novel exon was engineered to contain the Kozak sequence and AUG start codon (Fig. 1f). All possible downstream start codons were also removed to ensure that an AUG start would be included in response to LMI070 binding only. Increased luciferase expression was observed for each candidate cassette transfected into HEK293 cells in response to LMI070, with the *SF3B3*-on switch exhibiting a greater than 100-fold induction (Extended Data Fig. 3a, b), five times that of the 20-fold induction afforded by the indSMN2 minigene (Fig. 1b).

To assess background splicing from the engineered switch cassette, we performed two PCR assays. The LMI070-spliced-in exon was not detected when using primer pairs that bound the flanking exons, whereas a faint signal was observed when using primers binding within the novel exon sequence (Extended Data Fig. 3c). Thus, in the absence of LMI070, the alternative exon may be included in a small fraction of the transcripts, mirroring what was found in the Intropolis dataset. Overall, these assays showed marginal baseline luciferase activity in the absence of LMI070 for all candidate cassettes, which may reflect in-frame non-AUG start codon activity[12] (Extended Data Figs. 3b, 4). The SF3B3-on switch, which showed the least background splicing, was used in all subsequent studies and is hereafter referred to as X^{on}.

We first compared X^{on} induction from the Rous sarcoma virus (RSV), the phosphoglycerate kinase (PGK) and the minimal cytomegalovirus (mCMV) promoters. All promoters drove dose-responsive inducible expression that was mirrored by splicing (Fig. 1g, Extended Data Fig. 5). The induction strength was of the order PGK ≈ RSV > mCMV, thereby providing tools for a gradient of induction.

To assess X^{on} in vivo, eGFP was cloned into the cassette, validated in vitro (Extended Data Fig. 6a) and the construct packaged into AAV9. AAV9-X^{on}-eGFP was administered intravenously to mice, and 4 weeks later the mice were given a single oral dose of either vehicle or LMI070 and eGFP expression assessed 24 h later in the liver, heart and skeletal muscle (Fig. 2a). There was notable eGFP fluorescence in liver and heart sections (Fig. 2b, Extended Data Fig. 6b), and the dose response of the eGFP signal that was observed by microscopy was confirmed by western blot (Fig. 2c, Extended Data Fig. 6c), RT–qPCR and splicing assay (Fig. 2d, Extended Data Fig. 6d–f). Notably, eGFP protein levels and novel exon splicing correlated directly to the dose of LMI070.

We next tested the responsiveness of the X^{on} cassette to a second LMI070 dose. Mice were treated intravenously with AAV9-X^{on}-eGFP, and 4 weeks later were given one oral dose of vehicle or of LMI070. One day later, some of the mice were euthanized, and eGFP induction was assessed by histology, splicing and RT–qPCR assays. The remaining mice underwent one week of drug washout, after which they were given LMI070 or vehicle (Fig. 2e). Induction in the liver was evident after the first and the second dose by histology, western blot, splicing

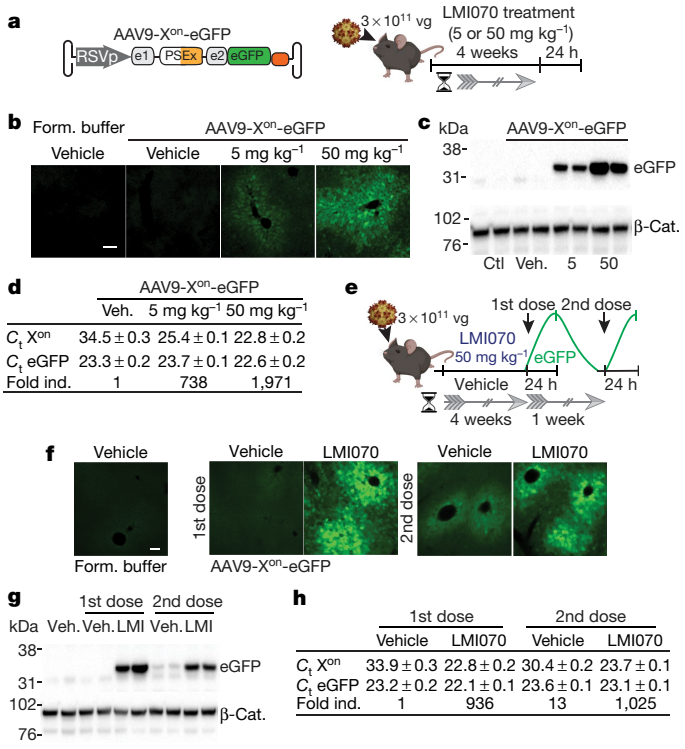

Fig. 2 | Activity of X^on in liver. a, Schematic of experiments using AAV9-X^on-eGFP. Mice were injected intravenously with AAV9-X^on-eGFP, after 4 weeks they were orally dosed once with LMI070, and tissues were collected 24 h later to assess mRNA (Extended Data Fig. 6) and protein expression. vg, viral genomes. **b**, Representative photomicrograph showing eGFP in the liver 24 h after dosing. $n = 3$ mice per group. Scale bar, 100 µm. **c**, Representative eGFP western blot with β-catenin (β-Cat.) as the loading control. $n = 4$ mice per group. Form. buffer, vector formulation buffer; Veh., vehicle. **d**, Average (mean ± s.e.m.) cycle threshold (C_t) values for eGFP or LMI070-induced expression using TaqMan assays (Extended Data Fig. 6e). The fold change stated for the spliced product is relative to vehicle-treated, AAV9-X^on-eGFP injected mice. $n = 4$ mice per group. **e**, Schematic of the re-dosing experiment. Mice were injected intravenously and 4 weeks later were dosed with LMI070 or vehicle. LMI070-treated mice were subjected to drug washout for one week and then redosed with drug or vehicle ($n = 5$ mice per group). Tissues were collected 24 h after each dose. **f**, Representative photomicrograph of the liver showing eGFP 24 h after each dose. $n = 2$ mice per group. Scale bar, 100 µm. **g**, Representative eGFP western blot 24 h after dosing, with β-catenin as loading control. $n = 3$ mice per group. **h**, Average (mean ± s.e.m.) C_t values for eGFP and fold change relative to AAV9-X^on-eGFP-injected mice treated with vehicle ($n = 3$ mice per group).

and RT–qPCR assays (Fig. 2f–h, Extended Data Fig. 6g, h). Induction in the skeletal muscle and the heart was also observed (Extended Data Fig. 6h, i), the relative levels of which were greatest for the latter (around 400-fold and 3,000-fold, respectively). Notably, the fold induction for each tissue was similar after each dose (Fig. 2h, Extended Data Fig. 6i). Cumulatively, these data show that eGFP expressed from an AAV-encoded X^on cassette remains undetectable in the uninduced state, and that LMI070 robustly induces expression.

We next assessed the efficacy of X^on for controlling erythropoietin (Epo), which is used to treat anaemia associated with chronic kidney disease[13]. The X^on cassette expressing mouse Epo (mEpo) was packaged in AAV8 (AAV8-X^on-Epo) and the construct was delivered intravenously to mice, which were subsequently treated with LMI070 or vehicle (Fig. 3a). mEpo plasma levels increased 25-fold to 62-fold in response to 2.5 or 10 mg kg^{-1} of LMI070, respectively, and returned to baseline 5 days after induction. One day after induction, Epo levels in AAV-eGFP or AAV-mEpo vehicle-treated mice were 173.6 ± 26 pg ml^{-1}

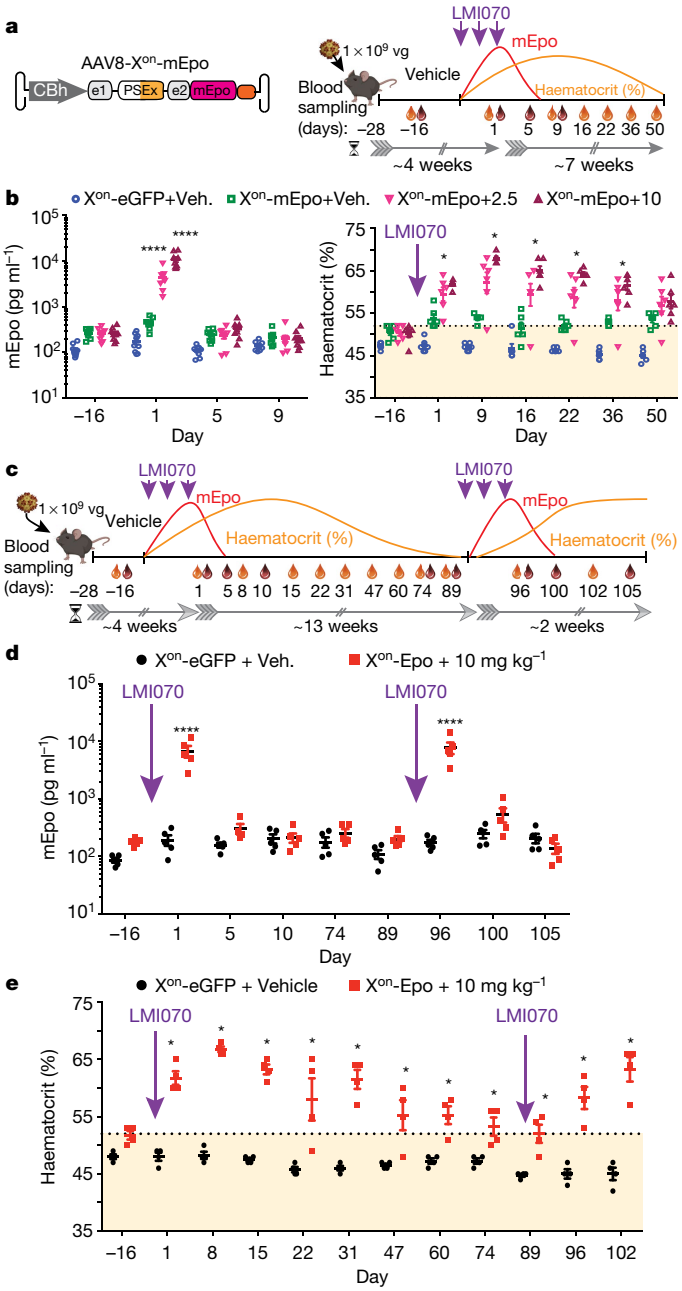

Fig. 3 | Drug-induced regulation of Epo. a, Experimental design for mEpo induction and the effect on haematocrit levels. Three weeks after AAV or buffer delivery, mice were dosed with vehicle or LMI070 at 2.5 or 10 mg kg^{-1} every other day for a total of 3 doses. Blood was collected for mEpo (red drop) and haematocrit (orange drop) assays as indicated. **b**, Left, mEpo levels 2 weeks after AAV injection, and 1, 5 and 9 days after the last dose. ****$P < 0.0001$, LMI070-treated versus vehicle-treated mice; ****$P < 0.0001$, 10 versus 2.5 mg kg^{-1} LMI070-treated mice. Right, haematocrit levels two weeks after AAV injection, and for 50 days after dosing. The orange shaded area shows the haematocrit range of wild-type mice. *$P < 0.05$ mEpo injected, LMI070-treated mice versus vehicle. **c**, Schematic of the re-inducibility experiment. X^on-mEpo-AAVs were delivered intravenously and mice given vehicle or LMI070 orally every other day for a total of 3 doses. After haematocrit returned to baseline levels, LMI070 was re-administered and mice were monitored as before. **d**, mEpo levels from 2 weeks after AAV delivery. ****$P < 0.0001$ AAV-X^on-mEpo-injected, LMI070-treated mice versus AAV-eGFP-injected mice. **e**, Haematocrit levels assessed over the time course of the experiment. *$P < 0.05$ mEpo-injected mice treated with LMI070 versus eGFP-injected mice. Data are mean ± s.e.m. of 9, 6 (**b**), 5 (**d**) or 4 (**e**) mice per group, significance was determined by two-way ANOVA followed by Bonferroni's post hoc test.

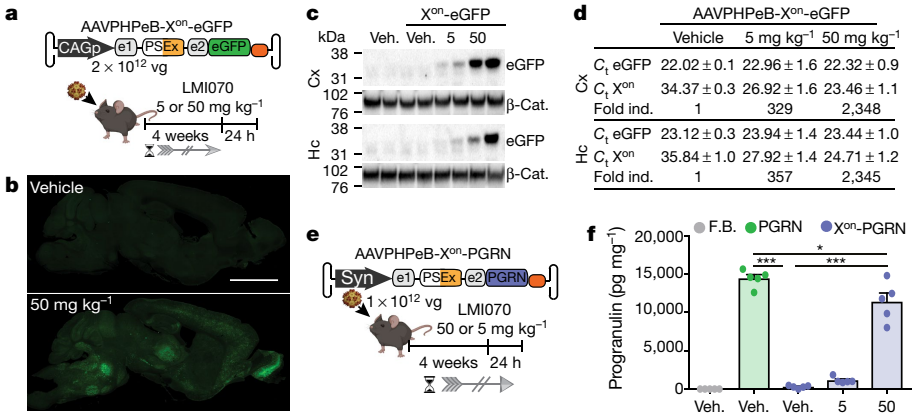

Fig. 4 | In vivo activity of X^{on} in the brain. a, Schematic of the AAVPHPeB-X^{on}-eGFP experiment. AAVs were injected intravenously, then after 4 weeks mice were given an oral dose of LMI070, and brains were collected 24 h later to assess splicing (Extended Data Fig. 7b), transcript levels and protein expression. **b**, Representative compiled photomicrographs (5 mice per group) from 40-µm-thick sagittal sections. Scale bar, 3 mm. **c**, Representative eGFP western blots of the cortex (Cx) and the hippocampus (Hc), with β-catenin as the loading control. $n = 3$ mice per group. **d**, Average (mean ± s.e.m.) C_t values for eGFP and fold change relative to AAV-X^{on}-eGFP-injected mice treated with vehicle. **e**, Schematic depicting the assessment of AAV-X^{on}-PGRN for regulation of progranulin expression in the brain. Vectors were administered intravenously, then after 4 weeks mice were treated with a single oral dose of LMI070 or vehicle, and tissues were collected 24 h later. **f**, Progranulin protein levels in the cortex. Data are mean ± s.e.m. of 5 mice per group. ***$P < 0.001$ for AAV-PGRN or AAV-X^{on}-PGRN + 50 mg kg^{-1} versus mice injected with AAV-X^{on}-PGRN + vehicle, *$P < 0.05$ for AAV-X^{on}-PGRN + 50 mg kg^{-1} versus AAV-PGRN, one-way ANOVA followed by Bonferroni's post hoc test. F.B., vector formulation buffer.

and 446 ± 40 pg ml^{-1}, respectively. For LMI070 treatment, mEpo levels increased in AAV8-X^{on}-mEpo mice to 4,333 ± 797 pg ml^{-1} or 10,870 ± 1,383 pg ml^{-1} for doses of 2.5 mg kg^{-1} or 10 mg kg^{-1}, respectively (Fig. 3b, left). The elevation of mEpo induced an increase in haematocrit to 60–70% above baseline levels depending on dose, after which a slow return to basal levels was observed (Fig. 3b, right).

We next tested the re-inducibility of AAV-X^{on}-mEpo in response to LMI070, as re-administrations are required for prolonged therapy in patients with chronic kidney disease (Fig. 3c). The re-induction of Epo generated similar results to the initial experiments, showing the practical utility of the X^{on} system for the regulation of therapeutic transgenes in response to repeat oral dosing (Fig. 3d, e).

To assess the applicability of our system for brain-targeted gene therapies, the X^{on}-eGFP cassette was packaged into AAVPHPeB[14] and delivered intravenously to mice (Fig. 4a). LMI070 induced robust eGFP expression throughout the brain, and all regions evaluated showed a clear dose response according to histological assessment (Fig. 4b, Extended Data Fig. 7a), western blot (Fig. 4c), RT–qPCR and splicing assays (Fig. 4d, Extended Data Fig. 7b).

Some gene-replacement therapies have only a narrow therapeutic expression window, including the expression of progranulin (PGRN) in the treatment of *PGRN*-deficient frontotemporal dementia and neuronal ceroid lipofuscinosis[15]. For X^{on}-regulated delivery of PGRN, AAVPHPeB-X^{on}-PGRN vectors were generated and administered intravenously to mice (Fig. 4e). Mice injected with AAVPHPeB vectors that constitutively express PGRN were used as a control. Although all groups showed similar *PGRN* mRNA levels after AAV injection (Extended Data Fig. 7c), PGRN protein was induced to levels of 1,135 ± 183 pg ml^{-1} and 11,393 ± 1,153 pg ml^{-1}, respectively, after LMI070 doses of 5 or 50 mg kg^{-1} (Fig. 4f). Splicing data were consistent with these results (Extended Data Fig. 7d).

It would be desirable to be able to regulate the expression of gene-editing proteins delivered by viral vectors. As such, we tested X^{on} for regulated *Staphylococcus aureus* Cas9 (SaCas9) editing in liver using Ai14 mice[16]. Because the X^{on}-SaCas9 cassette exceeds current AAV packaging limits (5.6 kb), we generated a smaller version that we denote miniX^{on} (Extended Data Fig. 8a). Induction and splicing of miniX^{on} was maintained and its overall amplitude was only modestly reduced relative to SF3B3-X^{on}; at 100 nM LMI070, induction of the miniX^{on} was 132-fold compared with 152-fold for X^{on} (Extended Data Fig. 8b, c). AAV8-miniX^{on}-SaCas9 plus single-guide RNAs targeting the *loxP*-STOP sequence in Ai14 mice were administered intravenously; after several weeks, LMI070 was administered and gene editing was assessed 7 days later (Extended Data Fig. 8d). The expression of tdTomato was detected by the fluorescence-activated cell sorting analysis of hepatocytes and histology on liver tissue sections (Extended Data Fig. 8e,f). Additionally, a genomic DNA PCR assay followed by Sanger sequencing confirmed gene editing (Extended Data Fig. 8g, h). Cumulatively, our results expand the utility of X^{on} to control Cas9 protein translation for gene-editing applications.

Substantial improvements have been made towards the development of small, potent, ubiquitous and tissue-specific promoters. However, the lack of efficient switches with which to fine-tune protein expression limits the broader application of gene therapy for disorders in which either loss of function or overexpression is consequential. Indeed, there are many clinical scenarios in which a narrow therapeutic window exists[15,17]. Moreover, toxicity can emerge as a result of sustained expression at supraphysiological levels. In AAV9 therapy for spinal muscular atrophy, the initial benefits of SMN overexpression were reversed by later toxicities caused by a splicing-machinery imbalance resulting from high levels of recombinant SMN in mice[18]. Although our work used AAV X^{on}, it could also be engineered for chimeric antigen receptor (CAR) T cell therapies and applied to the setting of CAR-T cell exhaustion[19] to pause CAR expression. Similarly, CRISPR-based treatments will benefit from using tunable switches, because refined control to provide a short burst of expression of CRISPR effector proteins would reduce unwanted off-target editing[20], and—because the proteins would be expressed for hours rather than for months or years—immune responses to nuclease-expressing cells would be limited[21,22]. Additionally, the transient exposure of cells to active nucleases should reduce the genomic integration of free AAVs that is seen upon prolonged expression of editing machinery[23].

Our switch system was originally designed for use with RG7800 or LMI070, but the refined system, X^{on}, was built around LMI070. Here we show that normally unspliced sequences that are rarely found in the transcriptome are spliced in in a dose-dependent manner. Although other splicing events induced by LMI070 represent potential drawbacks, we anticipate that most applications would entail infrequent

dosing, providing substantial periods of washout that would enable the re-expression of gene products that are silenced by the inclusion of suicide exons. Moreover, the X^{on} platform was developed using exons that were spliced in at very low drug exposures, further minimizing unwanted splicing events.

Most strategies for the control of gene expression have focused on controlling RNA levels by including *cis*-regulatory elements, although an approach to control protein translation—as is achieved with X^{on}—has been reported[24]. In this system, L7Ae controls translation through binding to a specific RNA motif[24]; however, immune responses could compromise clinical translation. For RNA regulation, ribozyme-based switches have been engineered to self-cleave mRNA sequences in which they were embedded[1]. Recently, optimization of a type-III hammerhead ribozyme has been reported, with higher self-cleavage activity and tighter regulation using morpholino-blocking oligomers for in vivo application[25]. However, morpholinos have a slow off-rate, which renders fine control problematic. Additionally, morpholinos do not reach the brain when delivered systemically. A tetracycline-responsive ribozyme switch that combines the hammerhead ribozyme N79 from *Schistosoma mansoni* with a tetracycline-binding aptamer showed tetracycline induction[26]. However, background expression was high. Another approach uses microRNA-binding sites within the 3′ untranslated region of exogenous mRNAs to reduce transcript stability in undesired cell types by co-opting the endogenous RNA interference machinery[27]. However, although this controls an off state, it would have to be merged with a switch such as X^{on} for precision in the on state.

The X^{on} switch demonstrates robust control of protein expression, with the extent of induction managed by dose and by promoter strength. In this system, decreasing protein-expression levels are entirely dependent on the half-life of the protein (more than 1 week for eGFP (Fig. 2g, Extended Data Fig. 6g) and less than 5 days for mEpo (Fig. 3b, d)). Merging X^{on} with protein domains targeted by proteolysis-targeting chimera molecules would provide another method to manage proteins with long half-lives[28]. Other possible improvements include adding an endoprotease site to the N-terminal region for fused miniexon sequence cleavage. Finally, we demonstrated control of CRISPR-effector protein induction using the X^{on} switch, and in combination with regulated intein splicing[29] or drug-dependent nuclear import[30], enhanced control of CRISPR activity could be further managed.

In summary, we present a simple, highly adaptable tool for regulated protein expression. We anticipate that this system could be adapted to any biological question or application in which the fine control of expression is desired.

Online content

Any methods, additional references, Nature Research reporting summaries, source data, extended data, supplementary information, acknowledgements, peer review information; details of author contributions and competing interests; and statements of data and code availability are available at https://doi.org/10.1038/s41586-021-03770-2.

1. Yen, L. et al. Exogenous control of mammalian gene expression through modulation of RNA self-cleavage. *Nature* **431**, 471–476 (2004).
2. Dow, L. E. et al. Inducible in vivo genome editing with CRISPR–Cas9. *Nat. Biotechnol.* **33**, 390–394 (2015).
3. Brown, B. D., Venneri, M. A., Zingale, A., Sergi Sergi, L. & Naldini, L. Endogenous microRNA regulation suppresses transgene expression in hematopoietic lineages and enables stable gene transfer. *Nat. Med.* **12**, 585–591 (2006).
4. Domenger, C. & Grimm, D. Next-generation AAV vectors—do not judge a virus (only) by its cover. *Hum. Mol. Genet.* **28** (R1), R3–R14 (2019).
5. Berget, S. M., Moore, C. & Sharp, P. A. Spliced segments at the 5′ terminus of adenovirus 2 late mRNA. *Proc. Natl Acad. Sci. USA* **74**, 3171–3175 (1977).
6. Cartegni, L. & Krainer, A. R. Disruption of an SF2/ASF-dependent exonic splicing enhancer in *SMN2* causes spinal muscular atrophy in the absence of *SMN1*. *Nat. Genet.* **30**, 377–384 (2002).
7. Naryshkin, N. A. et al. *SMN2* splicing modifiers improve motor function and longevity in mice with spinal muscular atrophy. *Science* **345**, 688–693 (2014).
8. Palacino, J. et al. SMN2 splice modulators enhance U1-pre-mRNA association and rescue SMA mice. *Nat. Chem. Biol.* **11**, 511–517 (2015).
9. *An Open Label Study Of LMI070 (Branaplam) in Type 1 Spinal Muscular Atrophy (SMA);* https://clinicaltrials.gov/ct2/show/NCT02268552
10. *FDA Approves Oral Treatment for Spinal Muscular Atrophy* (7 August 2020); https://www.fda.gov/news-events/press-announcements/fda-approves-oral-treatment-spinal-muscular-atrophy
11. Wang, J., Schultz, P. G. & Johnson, K. A. Mechanistic studies of a small-molecule modulator of SMN2 splicing. *Proc. Natl Acad. Sci. USA* **115**, E4604–E4612 (2018).
12. Ingolia, N. T., Ghaemmaghami, S., Newman, J. R. & Weissman, J. S. Genome-wide analysis in vivo of translation with nucleotide resolution using ribosome profiling. *Science* **324**, 218–223 (2009).
13. Eschbach, J. W., Kelly, M. R., Haley, N. R., Abels, R. I. & Adamson, J. W. Treatment of the anemia of progressive renal failure with recombinant human erythropoietin. *N. Engl. J. Med.* **321**, 158–163 (1989).
14. Chan, K. Y. et al. Engineered AAVs for efficient noninvasive gene delivery to the central and peripheral nervous systems. *Nat. Neurosci.* **20**, 1172–1179 (2017).
15. Amado, D. A. et al. AAV-mediated progranulin delivery to a mouse model of progranulin deficiency causes T cell-mediated toxicity. *Mol. Ther.* **27**, 465–478 (2019).
16. Madisen, L. et al. A robust and high-throughput Cre reporting and characterization system for the whole mouse brain. *Nat. Neurosci.* **13**, 133–140 (2010).
17. Collins, A. L. et al. Mild overexpression of MeCP2 causes a progressive neurological disorder in mice. *Hum. Mol. Genet.* **13**, 2679–2689 (2004).
18. Van Alstyne, M. et al. Gain of toxic function by long-term AAV9-mediated SMN overexpression in the sensorimotor circuit. *Nat. Neurosci.* **24**, 930–940 (2021).
19. Weber, E. W. et al. Transient rest restores functionality in exhausted CAR-T cells through epigenetic remodeling. *Science* **372**, eaba1786 (2021).
20. Fu, Y. et al. High-frequency off-target mutagenesis induced by CRISPR–Cas nucleases in human cells. *Nat. Biotechnol.* **31**, 822–826 (2013).
21. Charlesworth, C. T. et al. Identification of preexisting adaptive immunity to Cas9 proteins in humans. *Nat. Med.* **25**, 249–254 (2019).
22. Wagner, D. L. et al. High prevalence of *Streptococcus pyogenes* Cas9-reactive T cells within the adult human population. *Nat. Med.* **25**, 242–248 (2019).
23. Hanlon, K. S. et al. High levels of AAV vector integration into CRISPR-induced DNA breaks. *Nat. Commun.* **10**, 4439 (2019).
24. Saito, H. et al. Synthetic translational regulation by an L7Ae-kink-turn RNP switch. *Nat. Chem. Biol.* **6**, 71–78 (2010).
25. Zhong, G. et al. A reversible RNA on-switch that controls gene expression of AAV-delivered therapeutics in vivo. *Nat. Biotechnol.* **38**, 169–175 (2020).
26. Strobel, B. et al. A small-molecule-responsive riboswitch enables conditional induction of viral vector-mediated gene expression in mice. *ACS Synth. Biol.* **9**, 1292–1305 (2020).
27. Brown, B. D. et al. Endogenous microRNA can be broadly exploited to regulate transgene expression according to tissue, lineage and differentiation state. *Nat. Biotechnol.* **25**, 1457–1467 (2007).
28. Winter, G. E. et al. Phthalimide conjugation as a strategy for in vivo target protein degradation. *Science* **348**, 1376–1381 (2015).
29. Buskirk, A. R., Ong, Y. C., Gartner, Z. J. & Liu, D. R. Directed evolution of ligand dependence: small-molecule-activated protein splicing. *Proc. Natl Acad. Sci. USA* **101**, 10505–10510 (2004).
30. Roper, J. et al. In vivo genome editing and organoid transplantation models of colorectal cancer and metastasis. *Nat. Biotechnol.* **35**, 569–576 (2017).

Methods

Data reporting

No statistical methods were used to predetermine sample size. The in vitro and in vivo experiments were not randomized and the investigators performing molecular and biological studies were not blinded to treatment group. Individuals involved in tissue collection and histology were blinded to treatment group.

Cell culture, transfection and LMI070/RG7800 treatment

Human embryonic kidney (HEK293) cells (obtained from CHOP Research Vector Core stock) were maintained in DMEM media containing 10% fetal bovine serum (FBS), 1% L-glutamine and 1% penicillin/streptomycin at 37 °C with 5% CO_2. Cells were cultured in 24-well plates and transfected at 80–90% confluence using Lipofectamine 2000 transfection reagent, according to the manufacturer's protocol. For all experiments, 4 h after plasmid transfection, cells were treated with LMI070 (MedChemExpress, HY-19620, suspended in DMSO) or RG7800 (MedChemExpress, HY-101792A, suspended in H_2O) at the indicated concentrations. Cells were tested for mycoplasma by Research Vector Core. None of the lines used here are listed in the ICLAC database of commonly misidentified cell lines.

Plasmids, primers and custom-made TaqMan gene-expression assays

Sequences encoding X^{on} and miniX^{on} are available on the Davidson lab website https://www.thedavidsonlab.com and are deposited to Addgene (nos. 174659, 175660). All primer sequences and custom Taqman gene expression assays to determine *SF3B3* novel exon inclusion are available upon request. Primers and custom Taqman gene expression assays were obtained from Integrated DNA Technologies (IDT).

In vitro luciferase assays

HEK293 cells were cultured in DMEM (10% FBS (v/v), 1% penicillin/streptomycin (v/v) and 1% L-glutamine (v/v) in 24-well plates. At 70–80% confluence, cells were co-transfected with the X^{on}. Firefly luciferase cassettes (0.3 μg per well) and a SV40p-*Renilla* luciferase cassette as transfection control (0.02 μg per well). Four hours after transfection cells were treated with LMI070 or RG7800 at the indicated concentrations. At 24 hours post transfection, cells were rinsed with ice-cold PBS and *Renilla* and firefly luciferase activities were assessed using the Dual-Luciferase Reporter Assay System (Promega) as per the manufacturer's instructions. Luminescent readouts were obtained with a Monolight 3010 luminometer (Pharmigen). Relative light units (RLUs) were calculated as the quotient of *Renilla*/Firefly RLUs and results expressed relative to mock-treated control cells.

Mice and histology

Animal protocols were approved by The Children's Hospital of Philadelphia Institutional Animal Care and Use Committee. Five to six-week-old male C57BL/6J mice used in X^{on} studies to control translation of eGFP, mouse erythropoietin and human progranulin were obtained from Jackson Laboratories. Five to six-week-old male and female Ai14 mice used in gene-editing studies were obtained from an in-house-bred Ai14 colony derived from mice obtained from Jackson Laboratories (stock no 007914). AAV vectors were generated at the CHOP Research Vector Core, and were administrated by retro-orbital injection at 7–8 weeks old in a volume of 150–200 μl. For the dose–response studies, several weeks after AAV administration, a single dose of LMI070 at 2.5, 5, 10 or 50 mg kg^{-1} (MedChemExpress, HY-19620) or vehicle solution was administrated by oral gavage. For the re-dose studies, LMI070 was re-administrated at the indicated times and concentrations. At euthanasia, mice used for non-histology work were perfused with 0.9% cold saline mixed with 2-ml RNAlater (Ambion). Brains and liver samples were collected, flash-frozen in liquid nitrogen, and stored at −80 °C until use. For histological studies, mice were perfused with 15 ml ice-cold 0.1 M PBS followed by 15 ml 4% paraformaldehyde. Sections were analysed using a DM6000B Leica microscope equipped with a L5 ET filter cube (excitation and emission wavelengths of 470 ± 20 nm and 525 ± 15 nm, respectively; dichroic 495 nm), a 10X HC PLAPO (numerical aperture (NA) 0.40), and a 40X HC PLAPO CORR (NA 0.85) lens connected to a Sola Light Engine LED light source (Lumencor). Images were collected with a Hammatsu Orca flash 4.0 monochrome camera controlled, or Leica SP8 confocal microscope equipped with a white-light laser, HyD sensors, and 40X HC PL APO CS2 (NA 0.75) lens. The excitation and emission wavelengths were set at 493 and 497–535 nm or 554 and 563–730 nm for the green and red channels. The Leica LAS X (v.3.0.3) software was used for both controlling microscopes and obtaining images.

RNA extraction, RT–PCR and splicing assays

Total RNA was extracted using TRIzol (Life Technologies) according to the manufacturer's protocol, with the exception of 1 μl Glycoblue (Life Technologies) in addition to the aqueous phase in the isopropanol precipitation step and a single wash with cold 70% ethanol. To determine splicing of the SMN2-on and X^{on} switches, 2 μg of total RNA from HEK293 cells or tissue samples was treated with DNaseI Free kit (Thermo Fisher) followed by cDNA generation using the High capacity cDNA kit (Thermo Fisher). Splicing was determined by PCR using the Phusion HighFidelity polymerase (Thermo Fisher) and PCR products separated on a 2.5% agarose gel pre-stained with EtBr and spliced-in and spliced-out band densitometry performed using with the Chemi-Doc Imaging System (BioRad) and Image Lab analysis software. Splicing induction from mouse tissues was determined using two custom TaqMan assays designed to determine total or LMI070-spliced in mRNA transcripts. The percentage of induction was determined by dividing the average C_t novel exon and average C_t total, relative to control mice injected with AAV virus plus vehicle.

Genomic DNA extraction and genome-editing analysis

Genomic DNA from liver samples was extracted using a Monarch genomic DNA purification kit (NEB) according to the manufacturer's instructions. Deletion of the *loxP*-STOP-*loxP* region of the transgenic *ROSA26* locus in the Ai14 mice was confirmed by PCR using primers binding outside the intervening segment cleaved by the sgRNA/SaCas9 complex pair (forward: 5′-GCT GGT TAT TGT GCT GTC TCA TC-3′ and reverse: 5′-CAT GAA CTC TTT GAT GAC CTC CTC-3′). PCR products were cloned into TOPO plasmids using the TOPO TA Cloning Kit and subsequently transformed into DH5α competent cells. Individual colonies were analysed using Sanger sequencing to determine editing of the *loxP*-STOP cassette.

Western blots

Tissues were homogenized in RIPA buffer (final concentration: 50 mM Tris, 150 mM NaCl, 1% Triton-X100, 0.1% SDS, 0.5% sodium deoxycholate, with Complete protease inhibitors (Roche)) and samples were incubated for 1 h rotating at 4 °C then clarified by centrifugation at 10,000*g* for 10 min. Total protein concentration was determined by DC protein assay (BioRad) and 30 μg was loaded onto 4–12% NuPAGE Bis-tris gels in MES buffer (Novex Life Technologies) to determine eGFP and β-catenin levels. After electrophoresis, proteins were transferred to 0.2 μm PVDF (Bio-Rad). Membranes were blocked with 5% milk in PBS-T and then blotted with rabbit anti-β-catenin (Ab2365, dilution 1:4,000; Abcam), rabbit anti-GFP (A11122, dilution 1:5,000; Invitrogen) followed by horseradish-peroxidase-coupled antibodies (goat anti-rabbit: 111-035-144, dilution 1:50,000; Jackson ImmunoResearch). Blots were developed with ECL Plus reagents (Amersham Pharmacia) and imaged on the ChemiDoc Imaging System (BioRad). eGFP and β-catenin protein levels were determined using the same PVDF membrane (whole blot). Restore western blot stripping buffer (21063, Thermo Fisher Scientific) was used to remove primary eGFP and secondary antibodies before β-catenin detection.

Haematocrit and plasma epo assays

At each indicated time point, 70 µl of blood was collected from the eye into heparin-treated microhaematocrit capillary tubes (Fisher Scientific, 22-362-566) and centrifuged using a micro-haematocrit centrifuge (International Equipment Company model MB, 341118722). Haematocrit counts were then measured using a micro-haematocrit card reader (LW scientific, ZCP-EZRD-HEM7). Plasma samples in the capillary tubes were collected and stored at −80 °C. Two- or fourfold-diluted (control and vehicle treated mice, respectively) or tenfold-diluted plasma samples (LMI070 treated mice) were used for measuring plasma Epo protein concentration using a Mouse Erythropoietin Quantikine ELISA Kit (R&D), and ELISA samples measured with a SpectraMax M5 plate reader (Molecular Devices). The normal haematocrit range was obtained from ref. [31].

Quantification of human progranulin by time-resolved FRET immunoassay

Brain samples were homogenized with Precellys in 400 µl of STEN buffer (150 mM NaCl, 50 mM Tris-HCl, pH 7.6, 2 mM EDTA, 1% NP-40) with Complete Protease Inhibitor (Thermo, A32955) and PhosSTOP phosphatase inhibitor (Thermo, A32957). Brain extracts were then clarified by centrifugation for 20 min at 15,000 rpm at 4 °C. Supernatant was collected, and total protein concentration was quantified by BioRAD DC protein assay kit (Bio-Rad, 5000116). Samples were aliquoted and frozen at −80 °C for future use as needed. Human progranulin antibodies (R&D Systems AF2420 and R&D Systems MAG2420) were labelled with donor Tb-fluorophore and acceptor d2-fluorophore, respectively (Cisbio). After optimization of antibody titres and incubation conditions, quantification of human progranulin levels was performed in a 384-well low-volume ProxiPlate (Perkin Elmer, 6008238). Then, 16 µl of diluted sample was loaded in duplicate followed by the addition of 2 µl antibody mix. A standard curve was prepared using Recombinant Human Progranulin protein standard (R&D Systems, 2420-PG-050). All sample and standard dilutions were performed in 1× PBS with 0.1% bovine serum albumin. For brain tissue, the standard was spiked with STEN buffer homogenized mouse brain extract to account for the matrix effects. Plates were then incubated at room temperature for 1 h. Time-resolved fluorescence resonance energy transfer readout was performed with an EnVision Reader (PerkinElmer). After the excitation of the donor fluorophore Tb at 320 nm and a time delay of 100 µs, the resulting Tb and d2 emission signals were read at 615 nm and 665 nm, respectively.

Hepatocyte isolation and flow cytometry

To isolate hepatocytes from Ai14 mice, whole livers were perfused (perfusion solution: cold 0.5 mM EDTA in Ca^{2+}-, Mg^{2+}-free HBSS), excised and disrupted with forceps. They were then minced into very small pieces using a razor blade and enzymatically digested for 2 h at 37 °C with shaking (digestion solution: 3 mM $CaCl_2$, 200 units per ml collagenase IV, and 1.5% BSA in HBSS). The final hepatocyte suspension was passed through a 70-µm nylon mesh cell strainer and rinsed to finish straining cells through the filter (washing solution: 1.5% BSA in HBSS (Ca^{2+}, Mg^{2+}-, no phenol red). Cells were pelleted by centrifugation and washed, before fixation at room temperature for 15 min (fixing solution: 4% PFA in HBSS). Fixed cells were pelleted, resuspended in FACS buffer (0.5% BSA, EDTA (2 mM), in PBS), and counted using Trypan Blue (1:10 dilution) to determine the total count of live cells. For flow cytometry, cells were aliquoted and stained with primary (ASGR1, Proteintech, 11739-1-AP) and secondary (Alexa647, Thermo Fisher, A32733) antibodies, all diluted at 1:100 in 0.1% PBS/BSA for 30 min at room temperature. Flow cytometry data was acquired using a BD FACSAria Fusion (BD Biosciences). ASGR1/A647 fluorescence was detected using a 640-nm laser and a 670/30 filter. tdTomato fluorescence was detected using a 561-nm laser and a 582/15 filter. Data were analysed using FlowJo 10 software (FlowJo LLC).

RNA-seq

RNA-seq libraries were constructed using the Illumina TruSeq Stranded Total RNA with Ribozero gold protocol at the Iowa institute of Human Genomics. Data from four LMI070-treated (25 nM) and four DMSO-treated HEK293 cell groups were obtained after sequencing across two lanes run on an Illumina Hi-Seq 4000 150PE. The resulting fastq files were aligned to the GRCh38 human genome obtained from Ensembl using the STAR aligner[32]. Splice junction output by STAR were quantified using a custom R script designed to identify splicing events unique to LMI070 treatment. Top ranking LMI070-exclusive splice events were manually assessed for their applicability to function as a splicing switch. A primary requirement of this evaluation was that two splice events (donor and acceptor) were identified as exclusive or enriched in LMI070-treated cells creating inclusion of a pseudoexon of reasonable size. Candidate splice events were visually evaluated using the Sashimi plot function available in IGV[33–35]. Previously published RNA-seq results from ref. [8] (NVS-SM1 100nM, and DMSO) were obtained as fastq files from NCBI Gene Expression Omnibus. Splicing analysis was performed on these datasets using our analytical pipeline (as described above). NVS-SM1, also known as LMI070, induced splicing events from ref. [8] were compared against induced events obtained from our study. To assess the exclusivity of LMI070-induced splice sites to LMI070 treatment we evaluated the frequency with which candidate splice junctions were previously identified in diverse human RNA-seq datasets deposited in the Sequence Read Archive (SRA). This analysis was performed using Intropolis, a database of exon–exon junctions from 21,504 human RNA-seq samples in the SRA archive. The Intropolis database is indexed by GRCh37 genomic position so we first converted our GRCh38 positions to GRCh37 using the LiftOver tool from the UCSC genome browser[36]. We then queried LMI070-induced splice sites against the Intropolis database using a custom Python script. The results for each LMI070 candidate splice event are summarized in Extended Data Tables 1, 2. Differential gene expression analysis was performed using DESeq2 to compare samples from the LMI070 and DMSO conditions[37]. To visualize the abundance of meaningfully differentially expressed genes we generated a volcano plot with a Benjamini–Hochberg-adjusted *P* value threshold of 0.05 and a 0.1 log fold-change threshold.

Statistical analysis

Statistical analyses were performed using GraphPad Prism v.7 software. Outlier samples were detected using the Grubb's test ($\alpha = 0.05$). Normal distribution of the samples was determined using the D'Agostino and Pearson normality test. Data were analysed using one-way ANOVA or two-way ANOVA followed by a Bonferroni's post hoc test. Statistical significance was considered when $P < 0.05$. All results are shown as mean ± s.e.m.

Reporting summary

Further information on research design is available in the Nature Research Reporting Summary linked to this paper.

Data availability

RNA-seq datasets are archived in the NCBI Gene Expression Omnibus under accession number GSE176527. Sequences encoding X^{on} and $miniX^{on}$ along with primer sequences and details on the custom TaqMan gene expression assays to determine *SF3B3* novel exon inclusion are available on the Davidson lab website (https://www.thedavidsonlab.com). Plasmids encoding X^{on} and $miniX^{on}$ are available from Addgene (nos. 174659, 175660).

Code availability

The R code to characterize novel LMI070-induced splicing events from RNA-seq data is available at https://github.com/DavidsonLabCHOP/Xon.

31. O'Connell, K. E. et al. Practical murine hematopathology: a comparative review and implications for research. *Comp. Med*. **65**, 96–113 (2015).
32. Dobin, A. & Gingeras, T. R. Mapping RNA-seq reads with STAR. *Curr. Protoc. Bioinformatics* **51**, 11.14.1–11.14.19 (2015).
33. Thorvaldsdóttir, H., Robinson, J. T. & Mesirov, J. P. Integrative Genomics Viewer (IGV): high-performance genomics data visualization and exploration. *Brief. Bioinform*. **14**, 178–192 (2013).
34. Robinson, J. T. et al. Integrative genomics viewer. *Nat. Biotechnol*. **29**, 24–26 (2011).
35. Katz, Y. et al. Quantitative visualization of alternative exon expression from RNA-seq data. *Bioinformatics* **31**, 2400–2402 (2015).
36. Kent, W. J. et al. The human genome browser at UCSC. *Genome Res*. **12**, 996–1006 (2002).
37. Love, M. I., Huber, W. & Anders, S. Moderated estimation of fold change and dispersion for RNA-seq data with DESeq2. *Genome Biol*. **15**, 550 (2014).
38. Nellore, A. et al. Human splicing diversity and the extent of unannotated splice junctions across human RNA-seq samples on the Sequence Read Archive. *Genome Biol*. **17**, 266 (2016).
39. Kearse, M. G. & Wilusz, J. E. Non-AUG translation: a new start for protein synthesis in eukaryotes. *Genes Dev*. **31**, 1717–1731 (2017).

Acknowledgements We thank E. Lysenko, Z. Hilfinger and J. Weber of the Davidson laboratory, as well as N. Hoque of the Novartis Institute for Biomedical Research for technical assistance.

This work was supported in part by the Hereditary Disease Foundation (A.M.M. and P.T.R.), T32 HG009495 (National Institutes of Health) (P.T.R.), NBIR (R.S., D.L., A.M.M. and B.L.D.) and the Children's Hospital of Philadelphia Research Institute.

Author contributions A.M.M. designed the research, performed experiments, analysed data and wrote the manuscript. A.A.H., E.L. and D.L. performed experiments. P.T.R. performed all bioinformatic analyses and wrote the manuscript. L.T. performed all histology analysis and contributed to statistical analyses. A.M. contributed to all in vivo studies. R.S. and D.L. assisted with progranulin studies. B.L.D. designed and supervised the research, analysed data and wrote the manuscript.

Competing interests B.L.D. serves on the advisory boards and/or has sponsored research from Homology Medicines, Intellia Therapeutics, Spirovant Sciences, Resilience Bio, Patch Bio, Saliogen, Moment Bio, Triplet Biosciences, Panorama Medicines, Roche and NBIR. A.M.M. has sponsored research from NBIR.

Additional information

Supplementary information The online version contains supplementary material available at https://doi.org/10.1038/s41586-021-03770-2.

Correspondence and requests for materials should be addressed to A.M.M. or B.L.D.

Peer review information *Nature* thanks Alessandra Biffi, Mikhail Shapiro and the other, anonymous, reviewer(s) for their contribution to the peer review of this work.

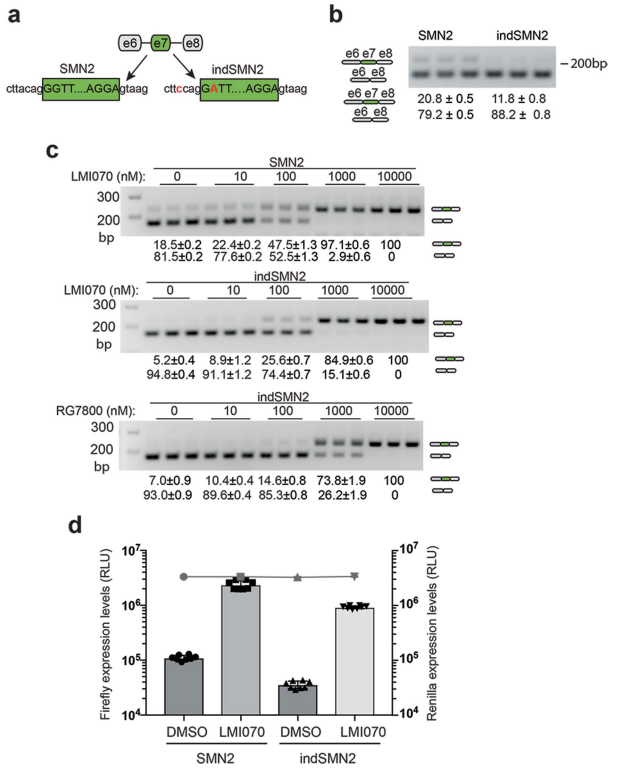

Extended Data Fig. 1 | In vitro assessment of SMN2-on cassettes. a, Cartoon depicting *SMN2* exon 7 in its native sequence or with splice-site modifications introduced to reduce background levels of exon 7 inclusion (3′ acceptor splice site, indSMN2). **b**, Representative RT–PCR reaction showing exon 7 inclusion with the SMN2-on cassettes in the absence of LMI070. The quantification of the exon 7 spliced-in or -out transcripts is depicted as the mean ± s.e.m. of 6 biological replicates. **c**, Exon 7 splicing of the SMN2 and indSMN2 cassette in response to LMI070 or RG7800. Representative RT–PCR reaction showing exon 7 inclusion as a function of LMI070 or RG7800 dose. The quantification of the exon 7 spliced-in or spliced-out transcripts are the relative transcript levels presented as the mean ± s.e.m. of 8 biological replicates. **d**, Luciferase activity of the SMN2 and indSMN2 cassettes in response to LMI070. The graph shows relative expression of firefly luciferase expressed from the SMN2-on or indSMN2-on cassettes in cells treated with DMSO or LMI070 (100 nM). The activity of the transfection control *Renilla* luciferase cassette is represented as a line above the bar graph. Data are the mean ± s.e.m. of 8 biological replicates.

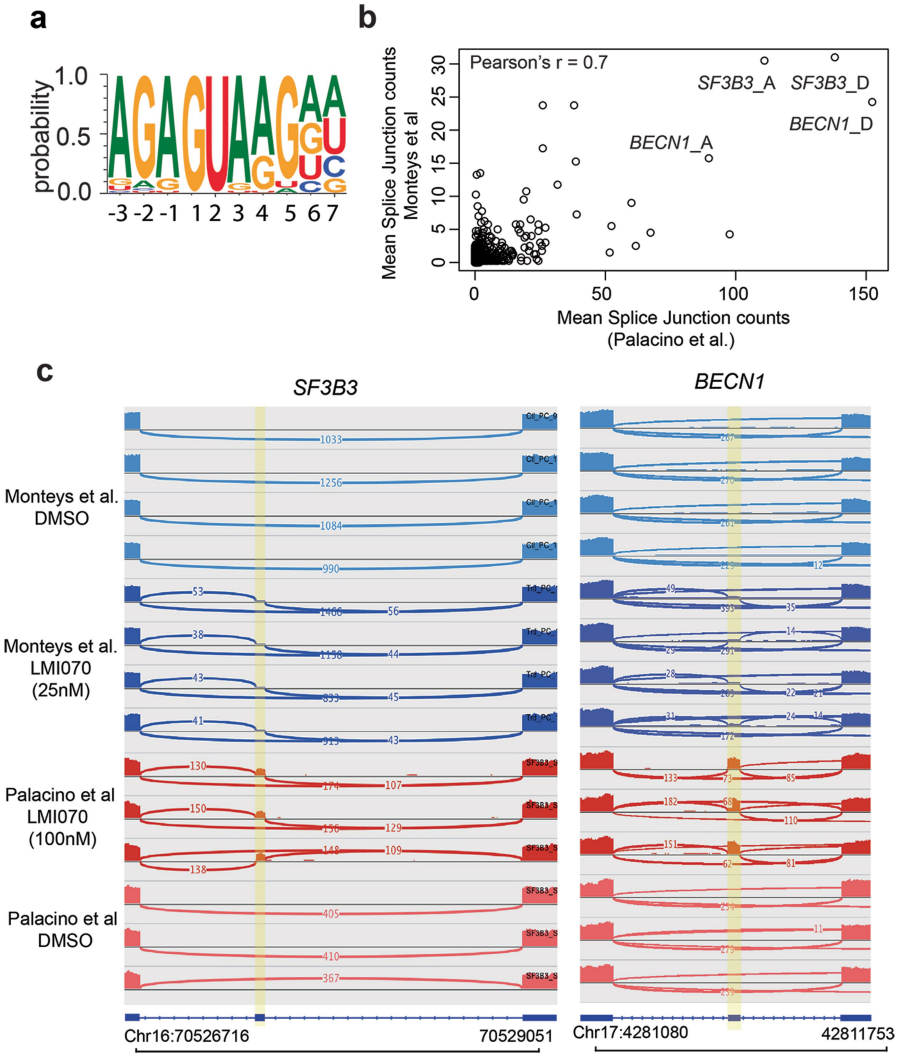

Extended Data Fig. 2 | Comparison between induced splice junctions in a previous study and in this work. See ref. [8]. **a**, Sequence logo of U1 RNA site targeted by LMI070 from 45 spliced-in exons identified by RNA-seq. **b**, To identify splice junctions with the highest induction across both studies we plotted the mean splice junction counts from our study against the mean splice junction counts from the dataset in ref. [8] reprocessed using our pipeline. The datasets correlate with Pearson's $r = 0.7$, indicating that induced junctions performed similarly by rank across both datasets. Additionally, the top ranked splice junctions associated with *SF3B3* and *BECN1* were consistent across both datasets. **c**, Sashimi plots depicting novel LMI070-spliced in exons for the *SF3B3* and *BECN1* genes identified in our study and in ref. [8] by RNA-seq. Genomic location, position of the LMI070 spliced in exon, and intronic counts observed are indicated.

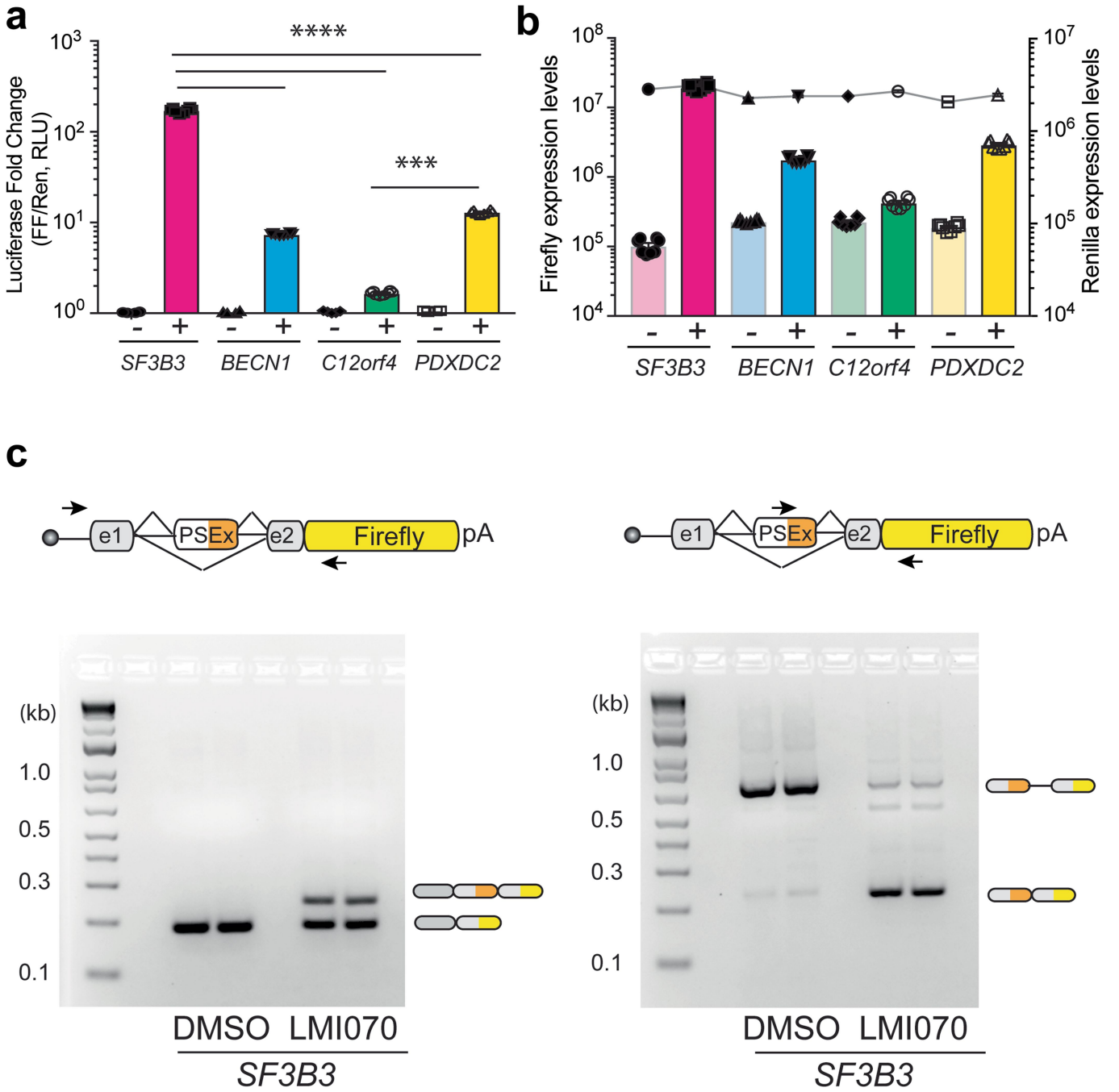

Extended Data Fig. 3 | Candidate minigene cassette responsiveness to LMI070 and splicing response to LMI070 of the SF3B3-X^{on} cassette. **a**, Luciferase induction of the minigene cassettes for *SF3B3*, *BECN1*, *C12ORF4* and *PDXDC2*. The fold-change luciferase activity in LMI070-treated samples (depicted as +) is relative to DMSO-treated (depicted as −) cells, with data normalized to *Renilla* luciferase expression. Data are the mean ± s.e.m. of 8 biological replicates. ****$P < 0.0001$ for *SF3B3* versus other candidate exons, ***$P < 0.001$ *C12orf4* versus *PDXDC2*, one-way ANOVA with Bonferroni's post hoc test. **b**, Luciferase activity of the minigene cassettes for *SF3B3*, *BECN1*, *C12ORF4* and *PDXDC2*. Data show expression of firefly luciferase from the minigenes in response to DMSO (−) or LMI070 (+) treatment relative to *Renilla* luciferase activity. Data are mean ± s.e.m. of 8 biological replicates. **c**, Splicing analysis of the *SF3B3*-X^{on} cassette. Representative RT–PCR splicing assay (6 biological replicates) showing inclusion of the LMI070-induced *SF3B3* exon in response to DMSO or LMI070 treatment. Inclusion of the LMI070 spliced-in exon was detected using primers binding the exons flanking the LMI070-induced exon (left), or using primers binding within the novel exon sequence (right).

a

Codons:	AUG	>>CUG	>>GUG	>ACG	>AUU=AUA	>UUG=AUC	>AAG=AGG
Frequency:	100	19	9	7	3	3	2	2	0.5	0.5

b

Non-AUG start codons in candidate minigene switches.

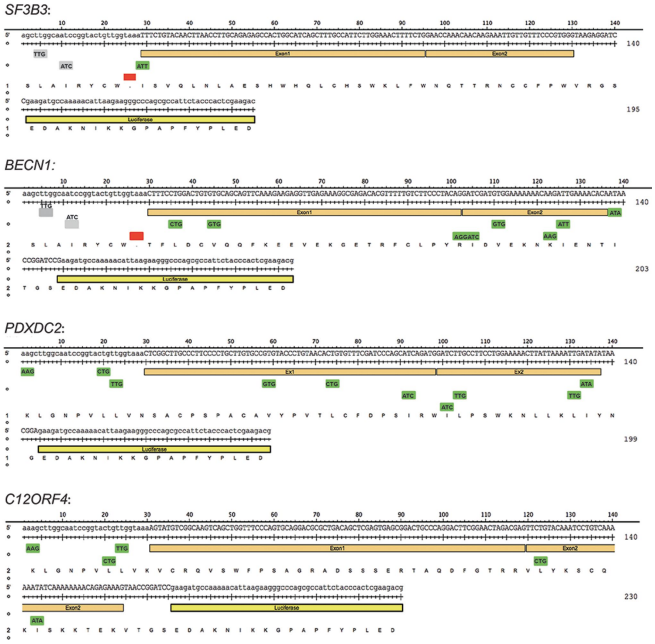

Extended Data Fig. 4 | Depiction of the frequency that non-AUG start codons are used determined by ribosome profiling. a, Translation frequency from AUG and non-AUG start codons determined from ribosome profiling[39]. **b**, Depiction of non-AUG start codons in frame luciferase transcripts expressed under control of the *SF3B3*, *BECN1*, *C12orf4* or *PDXDC2* minigenes.

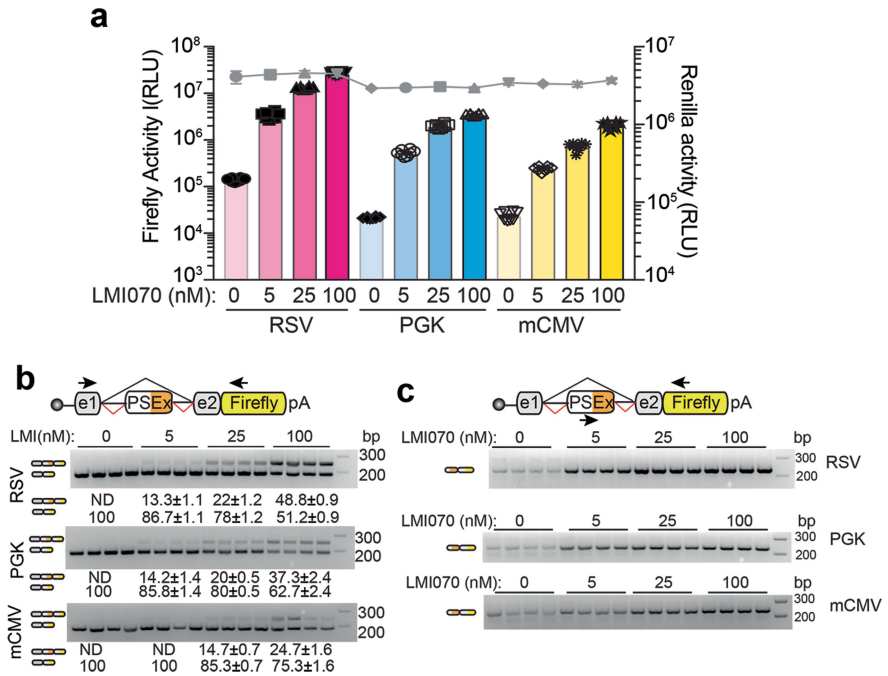

Extended Data Fig. 5 | Analysis of SF3B3-X^{on} expressed from different promoters. a, Firefly luciferase of the X^{on} cassettes in response to varying doses of LMI070 relative to *Renilla* luciferase (grey line). The data are the mean ± s.e.m. of 8 biological replicates. **b**, Representative RT–PCR for assessment of LMI070-induced pseudo exon expression. Exon inclusion in the X^{on} cassette was detected using primers flanking the pseudo exon. Data are the mean ± s.e.m. of 8 biological replicates. **c**, Representative gels from RT–PCR analysis for assessment of the LMI070-induced pseudo exons expressed from the noted promoters in response to varying doses of LMI070. Pseudo exon inclusion was detected using primers binding within the LMI070-induced pseudo exon and the downstream exon. Splicing was quantified and transcript levels presented as the mean ± s.e.m. of 8 biological replicates.

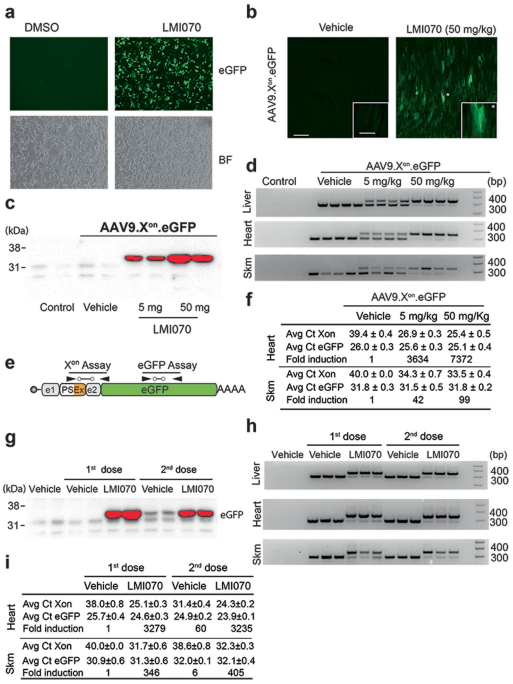

Extended Data Fig. 6 | Assessment of the SF3B3-X^{on} cassette to control translation of eGFP in vitro and in vivo. a, eGFP expression in HEK293 cells transfected with the SF3B3 minigene cassette (SF3B3-X^{on}-eGFP) and treated 24 h later with DMSO (left) or LMI070 (right). Bright-field panels are shown below (4 technical replicates). **b**, Representative photomicrograph of heart tissue sections showing eGFP in heart 24 h after treatment with LMI070 at 50 mg kg^{-1} ($n = 2$ mice). Scale bar, 200 µm. Inset, eGFP expression in cardiomyocytes at a higher magnification. Scale bar, 50 µm. **c**, Extended exposure of the western blot from Fig. 2c (4 mice per group). **d**, PCR assay demonstrates splicing activity in liver, heart and skeletal muscle in response to LMI070 (4 mice per group). **e**, Cartoon depiction of the X^{on} assays designed to quantify the LMI070-induced transcripts and eGFP expression levels from the X^{on} cassette after AAV9-X^{on}-eGFP gene transfer. **f**, Data show average C_t values for eGFP or LMI070-induced expression in heart and skeletal muscle. Fold change of the spliced-in expression cassette is shown relative to basal levels in mice injected with AAV9-X^{on}-eGFP and treated with vehicle (4 mice per group). **g**, Extended exposure of the western blot from Fig. 2h (3 mice per group). **h**, PCR assay demonstrates splicing activity in liver, heart and skeletal muscle after each LMI070 dose (3 mice per group). **i**, Data show average C_t values for eGFP or LMI070-induced expression in heart and skeletal muscle after each dose. Fold change of the spliced expression cassette is shown relative to basal levels in mice injected with AAV9-X^{on}-eGFP and treated with vehicle (3 mice per group).

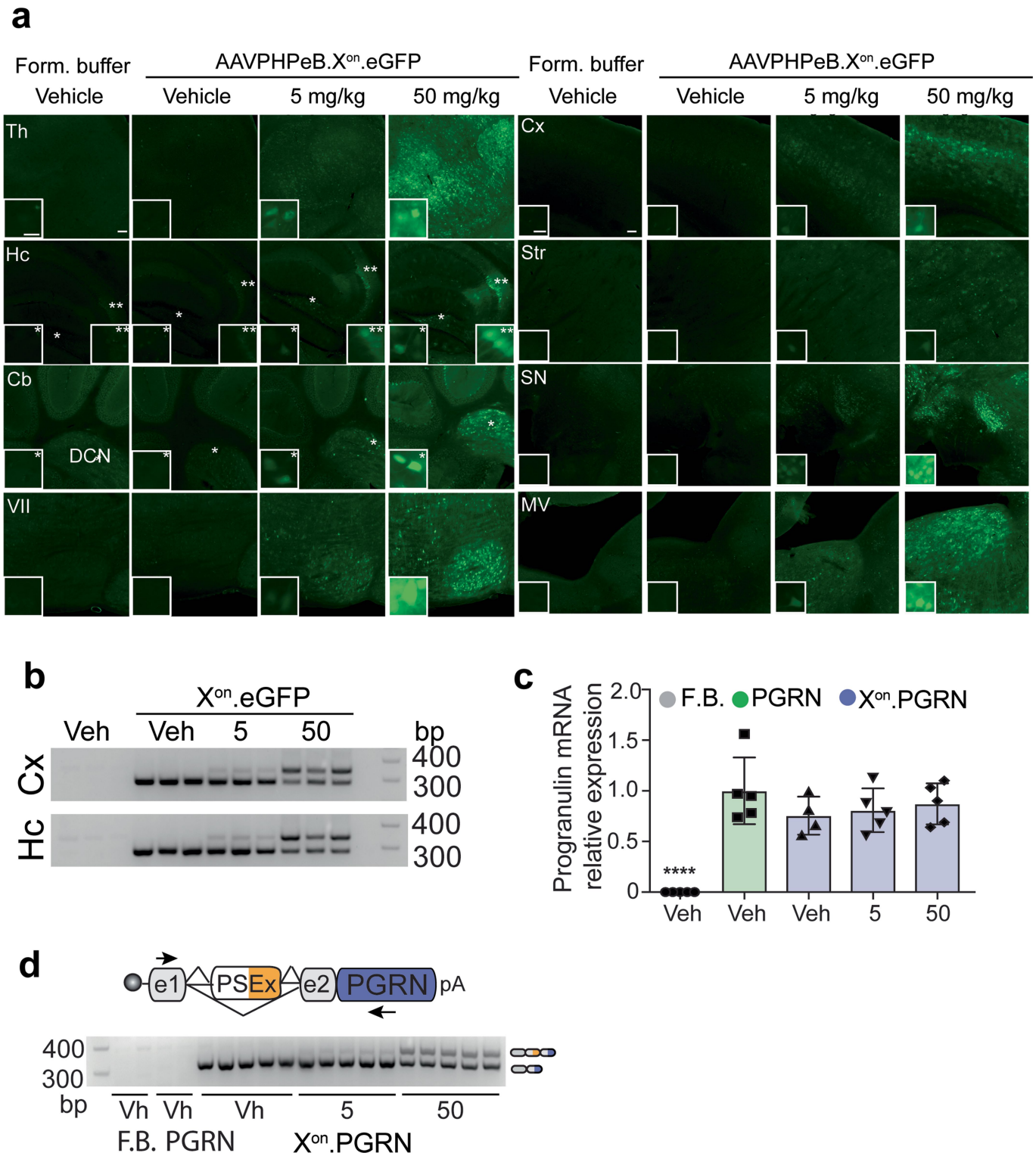

Extended Data Fig. 7 | In vivo activity of X^{on} in brain. a, Representative photomicrographs (5 mice per group) showing eGFP expression from mice treated intravenously 4 weeks earlier with AAVPHPeB-X^{on}-eGFP, and 24 h after treatment with vehicle or LMI070 at 5 or 50 mg kg^{-1}. Thalamus (Th), hippocampus (Hc), cerebellum (Cb) and facial motor nucleus (VII), cortex (Cx), striatum (Str), substantia nigra (SN), and medial vestibular nucleus (MV) are shown. Scale bar, 100 µm; inset scale bar, 25 µm. In the hippocampus, * and ** denote the polymorphic and CA3 areas, respectively. In the cerebellum, * denotes the deep cerebellar nuclei. **b**, Splicing assays for exon inclusion in the cortex and the hippocampus of mice injected with AAVPHPeB-X^{on}-eGFP (3 mice per group). **c**, RT–qPCR of human progranulin expression. Data are mean ± s.e.m. of 5 mice per group, ****$P < 0.0001$ vehicle versus AAV-treated groups, one-way ANOVA followed by Bonferroni's post-hoc test. **d**, Splicing assays for exon inclusion in cortex samples of mice injected with AAVPHPeB-X^{on}-PGRN (3 mice per group).

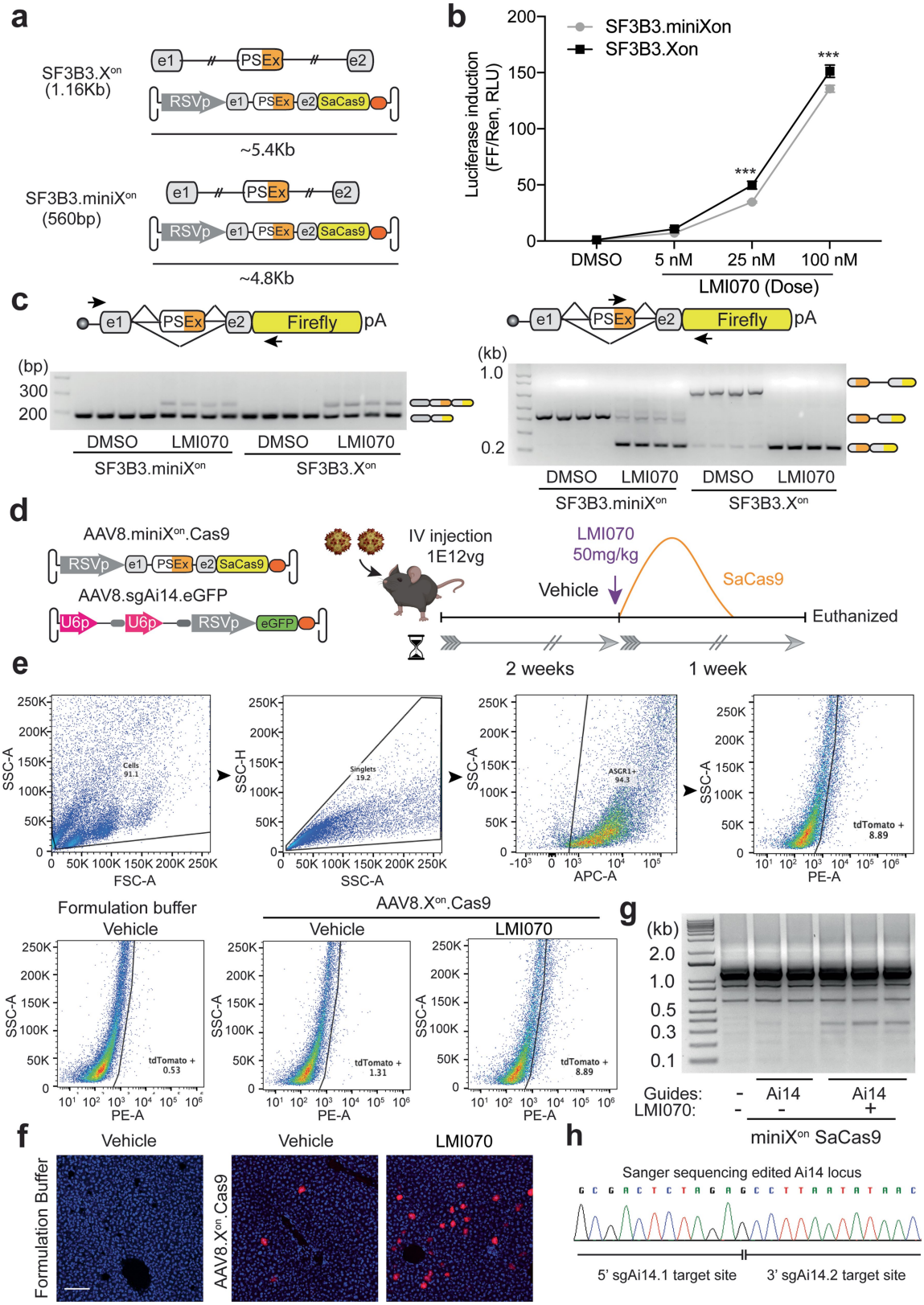

Extended Data Fig. 8 | See next page for caption.

Extended Data Fig. 8 | Generation of the miniX^{on} cassette and assessment of miniX^{on} control of SaCas9 for in vivo gene editing in liver. a, Cartoon depicting the AAV genome size with the SF3B3-X^{on} and SF3B3-miniX^{on} cassettes. **b**, Luciferase induction in HEK293 cells transfected with SF3B3-miniX^{on}-luciferase or SF3B3-X^{on}-luciferase in response to varying doses of LMI070. All samples are normalized to *Renilla* luciferase activity and are relative to DMSO treated cells. Data are the mean ± s.e.m. of 8 biological replicates (***$P < 0.001$ versus SF3B3.X^{on}, two-way ANOVA followed by Bonferroni's post hoc test). **c**, Splicing inclusion assays of the LMI070-induced exon at 100 nM LMI070. Pseudo exon inclusion in the X^{on} cassette was detected using primers flanking the pseudoexon (left) or by priming within the novel exon sequence (right; 4 technical replicates). **d**, Experimental design. Mice were injected with AAV8-miniX^{on}-SaCas9 plus AAV8-sgAi14-eGFP (1×10^{12} viral genomes, 1:1 ratio) and 2 weeks later dosed with vehicle or LMI070 at 50 mg kg^{-1} to induce SaCas9 expression and editing of the *loxP*-STOP cassette (guides: sgA14_1: 5′-CTCTAGAGTCGCAGATCCTC-3′, sgAi14_2: 5′-ACGAAGTTATATTAAGGGTT-3′). One week later, mice were euthanized, and livers processed to assess gene editing by genomic DNA PCR, histology and FACS of isolated hepatocytes. **e**, Representative FACS analysis of hepatocytes obtained from Ai14 mice after LMI070 or vehicle treatment. The gating/sorting strategy (above), and the percentage of tdTomato expressing cells for each condition (below) is shown (4 biological replicates). **f**, Representative photomicrographs of liver sections obtained from AAV injected Ai14 mice 1-week after LMI070 treatment. tdTomato expression (red) is evident in LMI070 treated mice (5 mice per group). Scale bars, 100 µm. **g**, SaCas9 mediated editing of the *loxP*-STOP cassette in Ai14 mice as detected by PCR assay of liver genomic DNA (3 of 5 mice with guides plus LMI, 2 of 4 mice with guides plus vehicle, 1 of 2 untreated mice are shown). A PCR product of 355 bp size corresponding to the edited Ai14 ROSA Locus was observed in the LMI070-treated mice. **h**, Sanger sequencing of the 355 bp PCR product confirmed targeted deletion of the *loxP*-STOP cassette and DNA repair of the Ai14 reporter locus.

Extended Data Table 1 | The genomic locations of candidate LMI070-induced exons and the frequency of events from RNA-seq datasets

		GRCh38				GRCh37 (hg19)		
	Gene ID	Genomic Minigene region	Pseudo exon position	DMSO Observed Avg Counts (J1, J2)	LMI070 Observed Avg Counts (J1, J2)	Genomic Minigene region	Pseudo exon position	LMI070 Binding sequence
Exclusive	*SF3B3*	chr16:70,526,657-70,529,199	chr16:70,527,376-70,527,429	0, 0	31, 30.5	chr16:70560560-70563102	chr16:70561279-70561332	AGAGTAAGAC
	BENC1	chr17:42,810,759-42,811,797	chr17:42,811,292-42,811,330	0, 0	24.45, 15.75	chr17:40962777-40963815	chr17:40963310-40963348	AGAGTAAGGC
	GXYLT1	chr12:42,087,786-42,097,614	chr12:42,095,151-42,095,214	0, 0	10.75, 23.75	chr12:42481588-42491416	chr12:42488953-42489016	AGAGTATAGT
	SKP1	chr5:134,173,809-134,177,053	chr5:134,175,284-134,175,385	0, 0	5.75, 23.75	chr5:133509500-133512744	chr5:133510975-133511076	AGAGTAGGAT
	SKP1	chr5:134,173,809-134,177,053	chr5:134,175,284-134,175,423	0, 0	15.25, 11.75	chr5:133509500-133512744	chr5:133510975-133511114	AGAGTAGGAT
	C12orf4	chr12:4,536,017-4,538,508	chr12:4,537,380-4,537,514	0, 0	17.5, 19	chr12:4645183-4647674	chr12:4646546-4646680	AGAGTAAGAA
	SSBP1	chr7:141,739,167-141,742,229	chr7: 141,741,310-141,741,459	0, 0	17.25, 2.25	chr7:141438967-141442029	chr7:141441110-141441259	AGAGTAAGGC
	RARS	chr5:168,517,815-168,519,190	chr5:168,518,369-168,518,523	0, 0	13.5, 1.5	chr5:167944820-167946195	chr5:167945374-167945528	AGAGTAGGAT
	RARS	chr5:168,517,815-168,519,190	chr5:168,518,469-168,518,523	0, 0	13.6, 1.75	chr5:167944820-167946195	chr5:167945474-167945528	AGAGTAGGAT
	PDXDC2P	chr16:70,030,988-70,031,968	chr16:70,031,186-70,031,248	0, 0	13.25, 10.25	chr16:70064891-70065871	chr16:70065089-70065151	AGAGTAAGAA
	STRADB	chr2:201,469,953-201,473,076	chr2:201,470,907-201,471,111	0, 0	9.5, 5.25	chr2:202334676-202337799	chr2:202335630-202335834	AGAGTAAGGA
	WNK1	chr12:894,562-896,732	chr12:895,161-895,196	0, 0	9, 5.5	chr12:1003728-1005898	chr12:1004327-1004362	AGAGTAGGTG
	WDR27	chr6:169,660,663-169,662,424	chr6:169,661,703-169,661,750	0, 0	8.5, 7.25	chr6:170060759-170062520	chr6:170061799-170061846	AGAGTAAGCA
	CIP2A	chr3:108,565,355-108,566,638	chr3:108,565,898-108,565,931	0, 0	7.75, 5	chr3:108284202-108285485	chr3:108284745-108284778	AGAGTAAGAA
	ITF57	chr3:108,191,521-108,206,696	chr3:108,192,476-108,192,526	0, 0	7.25, 5.25	chr3:107910368-107925543	chr3:107911323-107911373	AGAGTAGGCC
	HTT	chr4:3,212,555-3,214,145	chr4:3213622-3213736	0, 0	7, 2.25	chr4:3214282-3215872	chr4:3215349-3215463	AGAGTAAGGG
	SKA2	chr17:59,112,228-59,119,514	chr17:59119395-59119495	0, 0	6.75, 1	chr17:57189589-57196875	chr17:57196756-57196856	AGAGTAAGAG
	EVC	chr4:5,733,318-5,741,822	chr4:5741334-5741441	0, 0	6.5, 3	chr4:5735045-5743549	chr4:5743061-5743168	AGAGTAAGCA
	DYRK1A	chr21:37,420,144-37,473,056	chr21:37422581-37422652	0, 0	6.25, 6	chr21:38792446-38845358	chr21:38794883-38794954	AGAGTAGGTT
	GNAQ	chr9:77,814,652-77,923,557	chr9:77920648-77920703	0, 0	6, 1	chr9:80429568-80538473	chr9:80535564-80535619	AGAGTAAGCT
	ZMYM6	chr1:35,019,257-35,020,472	chr1:35020261-35020279	0, 0	5.75, 4	chr1:35484858-35486073	chr1:35485862-35485880	ACTGTGAGTA
	CYB5B	chr16:69,448,031-69,459,260	chr16:69448605-69448753	0, 0	5.75, 1.25	chr16:69481934-69493163	chr16:69482508-69482656	TAGGTGGTTC
	MMS22L	chr6:97,186,342-97,229,533	chr6:97201362-97201465	0, 0	5.75, 2	chr6:97634218-97677409	chr6:97649238-97649341	GAGGTGATTG
	MEMO1	chr2:31,883,262-31,892,301	chr2:31,887,035-31887087	0, 0	5, 2.25	chr2:32108331-32117370	chr2:32112104-32112156	AGAGTAAGGT
	PNISR	chr6:99,416,278-99,425,413	chr6:99420523-99420584	0, 0	5, 4	chr6:99864154-99873289	chr6:99868399-99868460	AGAGTAGTGT
Enriched	*CACNA2D1*	chr7:82,066,406-82,084,958	chr7:82,076,016-82,076,122	0.25, 0.75	18.5, 1.5	chr7:81695722-81714274	chr7:81705332-81705438	CAGGTTGGTA
	SSBP1	chr7:141,739,083-141,742,248	chr7:141741310-141741459	0.25, 0	16.75, 2.25	chr7:141438883-141442048	chr7:141441110-141441259	AGAGTAAGGC
	DDX42	chr17:63,805,048-63,806,672	chr17:63,806,151-63,805,994	0.25, 0	13.75, 4.5	chr17:61882408-61884032	Unable to lift over	AGAGTAAGAT
	ASAP1	chr8:130,159,817-130,167,688	chr8:130,160,785-130,160,793	0.25, 0.25	13, 11.5	chr8:131172063-131179934	chr8:131173031-131173039	AGAGTAAGTA
	DUXAP10	chr14:19,294,564-19,307,199	chr14:19,305,354-19,305,469	0.25, 0.75	9.5, 1.25	chr14:19882243-19894878	chr14:19893035-19893150	AGAGTAAGGT
	AVL9	chr7:32,558,783-32,570,372	chr7:32,562,558-32,562,913	0.25, 0.5	7.5, 1.5	chr7:32598395-32609984	chr7:32602170-32602525	AGAGTAAGAC
	DYRK1A	chr21:37,419,920-37,472,960	chr21:37,422,582-37,422,652	0.25, 0	6.25, 6	chr21:38792222-38845262	chr21:38794884-38794954	AGAGTAGGTT
	FAM3A	chrX:154,512,311-154,512,939	chrX: 154,512,568-154,512,706	0.25, 0	5.75, 1	chrX:153740635-153741263	chrX:153740892-153741030	GGGGTAGGGA
	FHOD3	chr18:36,740,620-36,742,886	chr18:36,742,377-36,742,468	0.5, 0.25	15.25, 3.5	chr18:34320583-34322849	chr18:34322340-34322431	AGAGTAAGAG
	*TBCA**	chr5:77,707,994-77,777,000	chr5:77,774,217	0.5	14	chr5:77003819-77072824	chr5:77070041	ND
	MZT1	chr13:72,718,939-72,727,611	chr13:72,725,642-72,725,778	0.5, 1	13.25, 1.25	chr13:73293077-73301749	chr13:73299780-73299916	AGAGTAAGAA
	LINC01296	chr14:19,092,877-19,096,652	chr14:19094556-19094671	0.5,	8.25,	chr14:19680556-19684333	chr14:19682237-19682352	AGAGTAAGAT
	SF3B3	chr16:70,541,627-70,544,553	chr16:70544169-70544249	0.5, 0	8.25, 3	chr16:70575530-70578456	chr16:70578072-70578152	AGAGTAAAGA
	SAFB	chr19:5,654,060-5,654,457	chr19:5,654,140-5,654,368	0.5, 0	6.25, 2	chr19:5654071-5654468	chr19:5654151-5654379	AGAGTAAGGA
	GCFC2	chr2:75,702,163-75,706,652	chr2:75,702,691-75,702,807	0.5, 0	6.25, 2	chr2:75929289-75933778	chr2:75929817-75929933	TGAGTAAGAG
	MRPL45	chr17:38,306,450-38,319,088	chr17:38,312,587-38,312,661	0.5, 0	5.75, 1.25	chr17:36462417-36474972	chr17:36468550-36468624	AGAGTAAGAC
	SPIDR	chr8:47,260,788-47,280,196	chr8:47,273,337-47,273,450	0.5, 0	5.5, 1.75	chr8:48173380-48192784	chr8:48185929-48186042	AGAGTAAGAC
	DUXAP8	chr22:15,815,315-15,828,713	chr22:15,817,119-15,817,234	0.75, 0.25	13.75, 1.25	chr14:19,680,685-19,691,354	chr14:19682237-19682352	AGAGTAAGAT
	PDXDC1	chr16:15,008,772-15,009,763	chr16:15,009,499-15,009,561	2, 1	16.75, 1.5	chr16:15102629-15103620	chr16:15103356-15103418	AGAGTAAGAA
	MAN1A2	chr1:117,442,104-117,461,030	chr1:117,456,085-117,456,206	0.75, 1	8, 5.25	chr1:117984726-118003652	chr1:117998707-117998828	AGAGTAAGGT
	RAF1	chr3:12,600,376-12,604,350	chr3:12,603,478-12,603,537	1, 0.25	16.5, 1	chr3:12641875-12645849	chr3:12644977-12645036	AGAGTAGGTA
	ERGIC3	chr20:35,548,787-35,554,452	chr20:35,549,163-35,549,207	1, 0	7.5, 2.5	chr20:34136540-34142223	chr20:34136917-34136961	GTGGTAGGTA

Summarized in this table are the differentially expressed candidate LMI070-induced splicing positions as identified by RNA-seq of HEK293 cells treated with either DMSO or LMI070 (25 nM). All candidates shown were manually selected from a bioinformatically generated list of top hits on the basis of their suitability for construction of an exon switching genomic minigene, their exclusivity to the LMI070 condition, and their minimal to undetectable levels in DMSO-treated cells. The top 25 rows (shaded green) indicate hits observed exclusively upon LMI070 exposure. The following 22 rows (shaded yellow) indicate candidates for which splicing was enriched but not totally exclusive to LMI070 treatment. Columns (from left to right) indicate: 1. Exclusivity to LMI070 induction. 2. The gene ID containing the splicing events of interest. 3. The GRCh38 genomic positions used to create the splice event-containing genomic minigene. 4. The GRCh38 genomic positions of the pseudo exon created by LMI070-induced splicing. 5. The average number of exon–exon junction spanning reads observed with DMSO treatment. 6. The average number of exon–exon junctions spanning reads observed with LMI070 treatment. To assess the frequency with which LMI070-induced events occur we queried Intropolis[38], a database containing the frequency of splicing events observed across 21,504 human RNA-seq samples, representing a diverse set of human tissues and conditions. The reference genome used for the Intropolis database is GRCh37 so the LiftOver feature from the UCSC genome browser was used to convert the GRCh38 coordinates to GRCh37. 7. The GRCh37 genomic position of the minigene. 8. The GRCh37 genomic position of the pseudo exon. 9. The DNA sequence of the LMI070 binding sequence in the pseudo exon.

Extended Data Table 2 | The genomic locations of candidate LMI070-induced exons and the frequency of events from RNA-seq datasets—continued

		GRCh37 (hg19)												
		Canonical Junction Metrics			LMI070 Junction1 Metrics					LMI070 Junction2 Metrics				
	Gene ID	CJ exon-exon juction	CJ Intropolis Datasets	CJ_Total Counts	J1 Position	J1 Num Datasets	J1 % Data Sets	J1 Total Counts	J1 % Total counts	J2 Positon	J2 Num Datasets	J2 % Data Sets	J2 Total Counts	J2 % Total counts
Exclusive	*SF3B3*	chr16:70560630-70562775	12873	825337	chr16:70560630-70561278	10	0.08	13	0.002	chr16:70561333-70562775	1	0.01	1	0.0001
	BENC1	chr17:40962947-40963672	13635	910210	chr17:40962947-40963309	301	2.21	552	0.061	chr17:40963349-40963672	182	1.33	303	0.0333
	GXYLT1	chr12:42481750-42491243	7430	43383	chr12:42481750-42488952	8	0.11	9	0.021	chr12:42489017-42491243	79	1.06	97	0.2236
	SKP1	chr5:133509714-133512545	13277	2756168	chr5:133509714-133510974	15	0.11	16	0.001	chr5:133511077-133512545	6	0.05	6	0.0002
	SKP1	chr5:133509714-133512545	13277	2756168	chr5:133509714-133510974	15	0.11	16	0.001	chr5:133511115-133512545	13	0.10	18	0.0007
	C12orf4	chr12:4645386-4647574	9856	102163	chr12:4645386-4646545	354	3.59	563	0.551	chr12:4646681-4647574	579	5.87	1102	1.0787
	SSBP1	chr7:141438991-141441968	14501	2473164	chr7:141438991-141441109	38	0.26	71	0.003	chr7:141441260-141441968	41	0.28	60	0.0024
	RARS	chr5:167945068-167946085	13602	826669	chr5:167945068-167945373	20	0.15	21	0.003	chr5:167945529-167946085	7	0.05	7	0.0008
	RARS	chr5:167945068-167946085	13602	826669	chr5:167945068-167945473	2	0.01	2	0.000	chr5:167945529-167946085	7	0.05	7	0.0008
	PDXDC2P	chr16:70064970-70065802	9586	117767	chr16:70064970-70065088	284	2.96	587	0.498	chr16:70065152-70065802	1097	11.44	3160	2.6833
	STRADB	chr2:202334776-202337677	9420	155599	chr2:202334776-202335629	150	1.59	189	0.121	chr2:202335835-202337677	171	1.82	260	0.1671
	WNK1	chr12:1003802-1005236	12935	800572	chr12:1003802-1004326	30	0.23	39	0.005	chr12:1004363-1005236	33	0.26	49	0.0061
	WDR27	chr6:170060863-170062399	9937	128203	chr6:170060863-170061798	1322	13.30	2407	1.877	chr6:170061847-170062399	960	9.66	1533	1.1958
	CIP2A	chr3:108284302-108285343	9210	124822	chr3:108284302-108284744	126	1.37	181	0.145	Not Found	Not Found	0.00	Not Found	0.0000
	ITF57	chr3:107910491-107925474	12662	583056	chr3:107910491-107911322	64	0.51	150	0.026	chr3:107911374-107925474	68	0.54	157	0.0269
	HTT	chr4:3214437-3215684	11146	243427	chr4:3214437-3215348	452	4.06	599	0.246	chr4:3215464-3215684	738	6.62	1064	0.4371
	SKA2	chr17:57189707-57196679	10377	297301	chr17:57189707-57196756	373	3.59	605	0.203	Not Found	Not Found	0.00	Not Found	0.0000
	EVC	chr4:5735163-5743442	6716	74348	chr4:5735163-5743060	86	1.28	120	0.161	chr4:5743169-5743442	107	1.59	154	0.2071
	DYRK1A	chr21:38792687-38844985	10821	152058	chr21:38792687-38794883	29	0.27	51	0.034	chr21:38794955-38844985	11	0.10	15	0.0099
	GNAQ	chr9:80430687-80537076	10041	224120	chr9:80430687-80535563	23	0.23	28	0.012	chr9:80535619-80537076	325	3.24	810	0.3614
	ZMYM6	chr1:35485204-35485983	11692	199379	chr1:35485204-35485861	312	2.67	1041	0.522	chr1:35485881-35485983	413	3.53	1465	0.7348
	CYB5B	chr16:69482048-69492995	13834	1150919	chr16:69482048-69482509	191	1.38	286	0.025	chr16:69482657-69492995	16	0.12	19	0.0017
	MMS22L	chr6:97634567-97676769	8959	91164	chr6:97634567-97649237	41	0.46	58	0.064	chr6:97649343-97676769	128	1.43	185	0.2029
	MEMO1	chr2:32108532-32117060	8678	99228	chr2:32108532-32112103	167	1.92	230	0.232	chr2:32112157-32117060	1010	11.64	1589	1.6014
	PNISR	chr6:99864305-99873090	13184	888372	chr6:99864305-99868398	1	0.01	1	0.000	chr6:99868461-99873090	21	0.16	29	0.0033
Enriched	*CACNA2D1*	chr7:81695841-81714084	6256	96528	chr7:81695841-81705331	1	0.02	1	0.001	chr7:81705439-81713748	2	0.03	7	0.0073
	SSBP1	chr7:141438991-141441968	14501	2473164	chr7:141438991-141441109	38	0.26	71	0.003	chr7:141441260-141441968	41	0.28	60	0.0024
	DDX42	chr17:61882536-61883894	12718	722896	NA	NA	NA	NA	NA	NA	NA	NA	NA	NA
	ASAP1	chr8:131172211-131179781	11448	396871	chr8:131172211-131173030	2429	21.22	16818	4.238	chr8:131173040-131179781	2397	20.94	16510	4.1600
	DUXAP10	chr14:19884030-19894699	638	1502	Not Found	Not Found	0.00	Not Found	0.000	chr14:19893151-19894699	31	4.86	34	2.2636
	AVL9	chr7:32599077-32609631	11339	199392	chr7:32599077-32602169	2728	24.06	6204	3.111	chr7:32602526-32609631	811	7.15	1355	0.6796
	DYRK1A	chr21:38792687-38844985	10821	152058	chr21:38792687-38794883	29	0.27	51	0.034	chr21:38794955-38844985	11	0.10	15	0.0099
	FAM3A	chrX:153740736-153741146	9459	98652	chrX:153740736-153740891	351	3.71	481	0.488	chrX:153741031-153741146	1834	19.39	3467	3.5144
	FHOD3	chr18:34320802-34322699	7279	113308	chr18:34320802-34322339	210	2.89	295	0.260	chr18:34322432-34322699	170	2.34	216	0.1906
	*TBCA**	chr5:77004173-77072028	14180	942768	NA	NA	NA	NA	NA	chr5:77070042-77072028	1306	9.21	4838	0.5132
	MZT1	chr13:73293236-73301661	12409	516948	chr13:73293236-73299779	51	0.41	103	0.020	chr13:73299917-73301661	51	0.41	79	0.0153
	LINC01296	chr14:19680686-19683691	239	315	chr14:19680686-19682236	20	8.37	22	6.984	chr14:19682353-19683691	1	0.42	1	0.3175
	SF3B3	chr16:70575738-70578340	12928	880623	chr16:70575738-70578071	233	1.80	467	0.053	chr16:70578153-70578340	174	1.35	273	0.0310
	SAFB	chr19:5654212-5654378	13168	1083231	Not Found	Not Found	0.00	Not Found	0.000	Not Found	Not Found	0.00	Not Found	0.0000
	GCFC2	chr2:75929550-75933648	11225	168121	chr2:75929550-75929816	124	1.10	195	0.116	chr2:75929934-75933648	534	4.76	697	0.4146
	MRPL45	chr17:36462599-36474585	12718	608565	chr17:36462599-36468549	778	6.12	1191	0.196	chr17:36468625-36474585	847	6.66	1292	0.2123
	SPIDR	chr8:48173584-48192449	10729	158491	chr8:48173584-48185928	414	3.86	568	0.358	chr8:48186043-48192449	708	6.60	1131	0.7136
	DUXAP8	chr14:19680686-19683691	239	315	chr14:19680686-19682236	20	8.37	22	6.984	chr14:19682353-19683691	1	0.42	1	0.3175
	PDXDC1	chr16:15102705-15103537	12939	767189	chr16:15102705-15103355	1472	11.38	3778	0.492	chr16:15103419-15103537	116	0.90	190	0.0248
	MAN1A2	chr1:117984948-118003110	11582	229559	chr1:117984948-117998706	427	3.69	914	0.398	chr1:117998829-118003110	40	0.35	57	0.0248
	RAF1	chr3:12641915-12645634	12808	832362	chr3:12641915-12644976	1841	14.37	4800	0.577	chr3:12645037-12645634	2187	17.08	5789	0.6955
	ERGIC3	chr20:34136619-34142142	4423	84287	chr20:34136619-34136916	2778	62.81	7045	8.358	chr20:34136962-34142142	194	4.39	922	1.0939

Columns (from left to right) indicate: 1. Exclusivity to LMI070 induction. 2. The gene ID containing the splicing events of interest. 3. The position of canonical splice junction (CJ). 4. The number of Intropolis RNA-seq datasets in which each canonical splice event was observed. 5. The total number of observations identified for each canonical splice site. 6. The position of junction 1 (J1) and the first LMI070-induced exon–exon junction (sorted by genomic position) connecting a canonical exon to a LMI070-induced pseudo exon. Columns 7 and 8 indicate the number and percentage of Intropolis datasets in which each J1 splice event was observed. Columns 9 and 10 indicate the number and percentage of total counts in which each J1 splice event was observed. 11. The position of junction 2 (J2) the second LMI070-induced exon–exon junction (sorted by genomic position) connecting a LMI070-induced pseudo exon to a canonical exon. Columns 12 and 13 list the number and percentage of Intropolis datasets in which the LMI070-induced splicing event was observed. Columns 14 and 15 indicate the total number and percentage of reads containing each junction in the Intropolis dataset.

Extended Data Table 3 | Comparison between disclosed hits in a previous study and in this work

gene	GRCh38	Splice Junction Found	baseMean	log2FoldChange	lfcSE	stat	pvalue	padj
ABHD10	chr3:111990700-111990751	3:111987052-111990699	9.809816136	0.614834912	0.466585174	1.317733495	0.187592878	0.999998084
ADAM12	chr10:126041344-126042235	Not Found						
AKT1	chr14:104793127-104793127	14:104792723-104793126	41.80684788	-0.26101857	0.231973571	-1.125208222	0.26050081	0.999998084
ANXA11	chr10:80180941-80181136	10:80176156-80180940	10.82449812	-0.218718834	0.42387425	-0.515999343	0.605854868	0.999998084
APLP2	**chr11:130123612-130123779**	**11:130122514-130123611**	**490.449954**	**0.356584851**	**0.084290488**	**4.230428123**	**2.33E-05**	**0.007262767**
APPL2	**chr12:105233091-105233405**	**Not Found**						
ARMCX6	**chrX:101617283-101617370**	**X:101616767-101617282**	**1.554115827**	**4.038853198**	**1.327731995**	**3.041919011**	**0.002350751**	**0.067486942**
		X:101616767-101617291	**1.979014083**	**4.34277536**	**1.312975149**	**3.307583822**	**0.000941045**	**0.043636072**
ATG5	chr6:106308364-106308491	6:106293107-106308363	172.1443391	-0.141439917	0.116742213	-1.211557606	0.225681771	0.999998084
AXIN1	chr16:291190-291297	16:289608-291189	12.88615371	0.567337279	0.398949658	1.422077369	0.155003792	0.986220545
BAIAP2	chr17:81110914-81110959	17:81108510-81110913	4.125817311	1.37672654	0.718313789	1.916608815	0.055287647	0.636240125
CCNB1IP1	chr14:20317794-20317974	Not Found						
CCT7	chr2:73235550-73235645	2:73234385-73235549	5.106947198	1.017231089	0.677438559	1.501584277	0.133204506	0.949522936
CEP57	chr11:95795516-95795559	11:95790744-95795515	14.58205551	-0.09994828	0.374087616	-0.267178799	0.789331499	0.999998084
CSF1	chr1:109926063-109926743	1:109925203-109926062	0.512925465	-2.527906075	1.798973282	-1.405193785	0.159963662	NA
DLGAP4	**chr20:36499242-36499321**	**20:36497067-36499241**	**2.321757283**	**4.629312735**	**1.234758303**	**3.7491651**	**0.000177424**	**0.019705473**
EPN1	chr19:55676625-55677218	19:55677219-55677549	6.792614573	0.137794309	0.548684186	0.251135923	0.801709023	0.999998084
EPN1	chr19:55677550-55677734	Not Found						
ERGIC3	**chr20:35554372-35554386**	**20:35548866-35554371**	**28.83410289**	**4.036660975**	**0.450049004**	**8.969380978**	**2.98E-19**	**1.36E-14**
		20:35549208-35554371	1.211236736	3.671748012	1.402133721	2.618686047	0.008826914	NA
FOXM1	chr12:2861299-2861412	12:2859664-2861298	10.02538278	1.393165926	0.478256758	2.913008346	0.00357965	0.083406816
GGCT	chr7:30497741-30497896	Not Found						
GRAMD3	chr5:126466294-126466336	5:119456369-119471635	11.26191388	0.47467429	0.423301943	1.121360999	0.26213423	0.999998084
HSD17B4	chr5:119471636-119471700	5:119457369-119471635	0.494108183	2.368999879	1.817387698	1.303519267	0.192397543	NA
LARP7	**chr4:112637644-112637787**	**4:112637240-112637643**	**27.19269642**	**3.451696147**	**0.399919423**	**8.630979006**	**6.08E-18**	**1.58E-13**
LARP7	chr4:112644425-112644488	4:112638674-112644424	0.728760441	2.934691979	1.612411811	1.820063558	0.068749326	NA
LRRC42	chr1:53947788-53947821	1:53946550-53947787	29.09604567	-0.664904577	0.265177179	-2.507397428	0.012162388	0.190363981
MADD	**chr11:47292543-47292596**	**11:47290817-47292542**	**2.731362466**	**4.872013188**	**1.210216484**	**4.025736926**	**5.68E-05**	**0.011525541**
MAN1B1	chr9:137088268-137088398	Not Found						
MRPL39	chr21:25587701-25587789	Not Found						
PCBP4	chr3:51962810-51962892	3:51961305-51962809	1.182311825	3.691518129	1.422245816	2.595555625	0.009443812	NA
		3:51962089-51962809	1.216301921	3.681908004	1.418185239	2.59621092	0.009425818	NA
PPHLN1	chr12:42351885-42352049	12:42335975-42351884	123.8298057	-0.046390515	0.135503904	-0.342355562	0.732083327	0.999998084
PRKACB	chr1:84144269-84144548	1:111619935-111627469	2.568291852	1.215471674	0.941010031	1.291667074	0.196472465	0.999998084
RAB23	chr6:57221319-57221459	Not Found						
RAP1A	chr1:111627470-111627563	Not Found						
RCC1	chr1:28518233-28518308	Not Found						
SREK1	chr5:66156065-66157740	5:66153597-66156064	33.02107777	-0.458074764	0.247829652	-1.848345265	0.064552411	0.697745988
SREK1	chr5:66158809-66158932	5:66153597-66158808	10.54393267	0.145262673	0.426009401	0.340984665	0.733115126	0.999998084
		5:66158231-66158808	7.253095127	-0.095361539	0.528821088	-0.180328548	0.856894645	0.999998084
STRN3	**chr14:30929201-30929311**	**14:30913658-30929200**	**50.93805874**	**0.932636289**	**0.216274269**	**4.312285011**	**1.62E-05**	**0.005970823**
STRN3	chr14:30918966-30919106	14:30919107-30929200	46.51202979	0.551658841	0.208079453	2.651193256	0.008020793	0.130401186
		14:30913658-30918965	55.45310576	0.329108298	0.20344735	1.617658317	0.105736254	0.881349323
TNRC6A	chr16:24758339-24758360	16:24750814-24758338	91.74639209	0.019177308	0.149159372	0.128569248	0.897698501	0.999998084

See ref. [8]. Column identity from left to right; Column A, Gene ID of genes containing a significantly induced exon as identified by Palacino et al.[8]; Column B, GRCh38 position of the induced exon; Column C, the associated splice junction of the identified induced exons, if found in our dataset 'splice junction found'; Columns D–I, Differential expression status of each splice junction in our dataset, DMSO ($n = 4$) versus 25 nM LMI070 ($n = 4$). Differential expression was performed using DESeq2. Column D, The mean of normalized counts for all samples 'baseMean'; Column E, the $\log_2$ fold change (maximum likelihood estimate) 'Log2FoldChange'; Column F, the associated standard error 'lfcSE'; Column G, the Wald statistic 'stat', Column H, the Wald test two-tailed *P* value 'p value'; Column I, the Benjamini–Hochberg (BH) multiple testing corrected *P* value "p adj". Genes observed to be significant ($P_{adj} < 0.05$) in our dataset are bolded.

nature research

Corresponding author(s): Davidson and Monteys

Last updated by author(s): Apr 30, 2021

Reporting Summary

Nature Research wishes to improve the reproducibility of the work that we publish. This form provides structure for consistency and transparency in reporting. For further information on Nature Research policies, see Authors & Referees and the Editorial Policy Checklist.

Statistics

For all statistical analyses, confirm that the following items are present in the figure legend, table legend, main text, or Methods section.

n/a	Confirmed
☐	☒ The exact sample size (*n*) for each experimental group/condition, given as a discrete number and unit of measurement
☐	☒ A statement on whether measurements were taken from distinct samples or whether the same sample was measured repeatedly
☐	☒ The statistical test(s) used AND whether they are one- or two-sided *Only common tests should be described solely by name; describe more complex techniques in the Methods section.*
☒	☐ A description of all covariates tested
☐	☒ A description of any assumptions or corrections, such as tests of normality and adjustment for multiple comparisons
☐	☒ A full description of the statistical parameters including central tendency (e.g. means) or other basic estimates (e.g. regression coefficient) AND variation (e.g. standard deviation) or associated estimates of uncertainty (e.g. confidence intervals)
☐	☒ For null hypothesis testing, the test statistic (e.g. *F*, *t*, *r*) with confidence intervals, effect sizes, degrees of freedom and *P* value noted *Give P values as exact values whenever suitable.*
☒	☐ For Bayesian analysis, information on the choice of priors and Markov chain Monte Carlo settings
☒	☐ For hierarchical and complex designs, identification of the appropriate level for tests and full reporting of outcomes
☐	☒ Estimates of effect sizes (e.g. Cohen's *d*, Pearson's *r*), indicating how they were calculated

Our web collection on statistics for biologists contains articles on many of the points above.

Software and code

Policy information about availability of computer code

Data collection	Images were collected using Leica LAS X (v.3.0.3) software. Description provided in the manuscript
Data analysis	All software is listed in the manuscript.

For manuscripts utilizing custom algorithms or software that are central to the research but not yet described in published literature, software must be made available to editors/reviewers. We strongly encourage code deposition in a community repository (e.g. GitHub). See the Nature Research guidelines for submitting code & software for further information.

Data

Policy information about availability of data

All manuscripts must include a data availability statement. This statement should provide the following information, where applicable:

- Accession codes, unique identifiers, or web links for publicly available datasets
- A list of figures that have associated raw data
- A description of any restrictions on data availability

Custom R and Python scripts are available on Github.
RNA-Seq datasets are archived in the NCBI Gene Expression Omnibus (GEO).

Field-specific reporting

Please select the one below that is the best fit for your research. If you are not sure, read the appropriate sections before making your selection.

☒ Life sciences ☐ Behavioural & social sciences ☐ Ecological, evolutionary & environmental sciences

For a reference copy of the document with all sections, see nature.com/documents/nr-reporting-summary-flat.pdf

Life sciences study design

All studies must disclose on these points even when the disclosure is negative.

Sample size	Sample sizes for each experiment are indicated in the figure legends
Data exclusions	Data were not excluded from the analysis
Replication	The number of biological or technical replicates are indicated in the figure legends for each experiment.
Randomization	The experiments were not randomized.
Blinding	Only histological analyses were performed in a double-blind manner.

Reporting for specific materials, systems and methods

We require information from authors about some types of materials, experimental systems and methods used in many studies. Here, indicate whether each material, system or method listed is relevant to your study. If you are not sure if a list item applies to your research, read the appropriate section before selecting a response.

Materials & experimental systems

n/a	Involved in the study
☐	☒ Antibodies
☐	☒ Eukaryotic cell lines
☒	☐ Palaeontology
☐	☒ Animals and other organisms
☒	☐ Human research participants
☒	☐ Clinical data

Methods

n/a	Involved in the study
☒	☐ ChIP-seq
☐	☒ Flow cytometry
☒	☐ MRI-based neuroimaging

Antibodies

Antibodies used	Rabbit anti-GFP antibody (Invitrogen; #A11122). Rabbit anti beta-catenin (Ab2365; Abcam). Goat anti-Rabbit (111-035-144, Jackson ImmunoResearch). anti-ASGR1 (11739-1-AP, Proteintech), Alexa647 (A32733, ThermoFisher). Human Progranulin Antibodies (AF2420 & MAS2420, R&D Systems)
Validation	All antibodies are commercially available and have been previously validated by the corresponding company.

Eukaryotic cell lines

Policy information about cell lines

Cell line source(s)	Human embryonic kidney (HEK293) cells were obtained from the Children's Hospital of Philadelphia Research Vector Core stock.
Authentication	None of the cells used were authenticated since they previously passed the quality controls of the Children's Hospital of Philadelphia Research Vector Core
Mycoplasma contamination	Cells were not tested for Mycoplasma by the investigators since they previously passed the quality controls of CHOP Research Vector Core
Commonly misidentified lines (See ICLAC register)	None of the cells used in the study were listed in ICLAC database of commonly misidentified cell lines.

Animals and other organisms

Policy information about studies involving animals; ARRIVE guidelines recommended for reporting animal research

Laboratory animals	Five/Six-week-old male C57Bl6/j mice were obtained from Jackson Laboratories (Bar Harbor, ME, USA). Five/Six-week-old Ai14 mice were previously obtained from Jackson Laboratories (Bar Harbor, ME, USA), and maintained in the laboratory by breeding with C57Bl6/j mice purchased from Jackson Laboratories.
Wild animals	The study did not involved wild animals.
Field-collected samples	The study did not involved samples collected from the field.
Ethics oversight	Animal protocols were approved by The Children's Hospital of Philadelphia Institutional Animal Care and Use Committee.

Note that full information on the approval of the study protocol must also be provided in the manuscript.

Flow Cytometry

Plots

Confirm that:

☒ The axis labels state the marker and fluorochrome used (e.g. CD4-FITC).

☒ The axis scales are clearly visible. Include numbers along axes only for bottom left plot of group (a 'group' is an analysis of identical markers).

☒ All plots are contour plots with outliers or pseudocolor plots.

☒ A numerical value for number of cells or percentage (with statistics) is provided.

Methodology

Sample preparation	Whole livers were perfused, excised, and minced in very small pieces using a razor blade and enzymatically digested for 2h at 37° C with shaking. The hepatocyte suspension was passed through a 70µm nylon mesh cell strainer. Cells were fixed in 4% PFA, pelleted and resuspended in FACS buffer before staining with the following antibodies: anti-ASGR1, Proteintech: 11739-1-AP (primary) and Alexa647,ThermoFisher: A32733(Secondary).
Instrument	Instrument used is BD FACSAria fusion.
Software	Data was collected with BD FACSDiva software, and data analyzed with FlowJo 10.7.1 software (FlowJo LLC)
Cell population abundance	The abundance of single cell hepatocyte population was >70%, as determined by flow cytometry.
Gating strategy	Liver single cell suspension was sorted for hepatocytes by gating on ASGR1-A647 positive signal. Positive edited hepatocytes were then gaited by tdTomato (PE-A) positive signal.

☒ Tick this box to confirm that a figure exemplifying the gating strategy is provided in the Supplementary Information.